Observations of Thick Disks in the Hubble Space Telescope Ultra Deep Field

Bruce G. Elmegreen[1], Debra Meloy Elmegreen[2]

ABSTRACT

The vertical profiles of chain and spiral galaxies in the Hubble Space Telescope Ultra Deep Field (UDF) are fit to $\mathrm{sech}^2\,(z/z_0)$ functions convolved with stellar profiles in order to measure the disk scale heights z_0 in four passbands. The bulge regions of the spirals are avoided. Photometric redshifts give absolute scales. The rms heights of the giant clumps in these galaxies are also measured. The results indicate that UDF disks are thick with an average $z_0 = 1.0 \pm 0.4$ kpc. The ratio of radial exponential scale length to z_0 is $\sim 3 \pm 1.5$. The scale heights are only 20% larger than the radii of the giant star-forming clumps and a factor of ~ 10 larger than the rms clump deviations around the midplanes. This suggests the clumps formed from midplane gas and dissolved to make the thick disks. Redshifted stellar population models suggest ages of ~ 1 Gy and mass column densities from 4 to 40 $\mathrm{M}_\odot$ pc^{-2}. The UDF disks look like young versions of modern thick disks. This resemblance is difficult to understand if galaxies grow over time or if subsequent accretion of thin disks gravitationally shrinks the observed thick disks. More likely, high redshift disks are thick because their mass column densities are low; a velocity dispersion of only 14 km s^{-1} reproduces the observed thickness. Modern thick disks require more heating at high redshift. This is possible if the gas that eventually makes the thin disk is in place before the youngest age of a modern thick disk, and if the existing stars are heated during the delivery of this gas.

Subject headings: galaxies: formation — galaxies: high-redshift — galaxies: spiral

[1]IBM Research Division, T.J. Watson Research Center, 1101 Kitchawan Road, Yorktown Heights, NY 10598; bge@watson.ibm.com

[2]Department of Physics & Astronomy, Vassar College, Poughkeepsie, NY 12604; elmegreen@vassar.edu

1. Introduction

The Milky Way (Gilmore & Reid 1983), other spiral galaxies (van der Kruit & Searle 1981a,b; Jensen & Thuan 1982; van Dokkum et al. 1994; Morrison et al. 1997; Pohlen et al. 2000; Dalcanton & Bernstein 2002, see Yoachim & Dalcanton 2006 and references therein), and S0 galaxies (Burstein 1979; Tsikoudi 1979; Pohlen, et al. 2004) have a thick disk component that is old and of moderate metallicity. In the Milky Way, it has a vertical velocity dispersion of $\sim 35 \pm 3$ km s^{-1} (Freeman 1987; Chiba & Beers 2000) and an exponential scale height between 600 pc (Chen et al. 2001) and 900 ± 300 (Buser et al. 1999; Ojha 2001; Kerber et al. 2001; Larsen & Humphreys 2003). The thin Milky Way disk is apparently a separate component (Carney et al. 1989; Chen et al. 2001). It varies in height from ~ 60 pc for the molecular gas (Cohen & Thaddeus 1977) to ~ 100 pc for the young stars to 330 pc for the old stars (Chen et al. 2001), with a corresponding increase in vertical velocity dispersion from ~ 8 km s^{-1} for molecular clouds (Stark & Brand 1989) to 20 km s^{-1} for old stars (Freeman 1987).

These differences in component age, velocity dispersion, metallicity, and scale height suggest several possible origins for galactic thick disks (see review in Wyse 2004): (1) they arise from gradual stochastic heating of stars that form in a thin disk (Wielen & Fuchs 1985; Fuchs et al. 2001); (2) they arise from sudden heating of thin disk stars during the impact of a smaller galaxy (Quinn et al. 1993; Mihos et al. 1995; Walker et al. 1996; Robin et al. 1996; Velazquez & White 1999; Aguerri et al. 2001); (3) they arise independently of thin disks as tidally stripped debris from companion galaxies (Gilmore et al. 2002; Abadi et al. 2003; Wyse et al. 2006); (4) they arise as a first step in the cooling of the disk from a highly turbulent initial condition (Eggen et al. 1962; Burkert, Truran, & Hensler 1992; Pardi, Ferrini, & Matteucci 1995; Brook et al. 2004, 2005, 2006); and (5) they arise from the dissolution of massive thin-disk clusters with small radii and large velocity dispersions (Kroupa 2002).

The distinct and homogeneous nature of thick disks (Seth et al. 2005; Mould 2005) suggests they were well mixed as they formed and that they stopped forming rather suddenly. This supports models involving an early phase of satellite and gas accretion, intense star formation, and vertical mixing that terminated around 6-9 Gy ago (when $z = 0.7 - 1.4$ in the standard ΛCDM model). Such accretion should also give thick disks a significant contribution from dissolved satellite remnants (Abadi et al. 2003).

The purpose of this paper is to examine the structure of young thick disks directly, using edge-on galaxies in the Hubble Space Telescope Ultra Deep Field (UDF). Reshetnikov, Dettmar, & Combes (2003) studied the Hubble Deep Field and noted that high redshift disks have thicker axial ratios than local galaxies. We found the same for spirals and chain galaxies

in the Tadpole Galaxy background field (Elmegreen, et al. 2004b, hereafter EEH04) and the UDF (Elmegreen & Elmegreen 2005, hereafter EE05; Elmegreen et al. 2005a; hereafter EERS). Here we measure the disk thicknesses, colors, and perpendicular color gradients of edge-on UDF galaxies using distances from photometric redshifts (Coe et al. 2006). We also measure the perpendicular sizes and rms deviations from the midplane of the giant star-forming clumps that typically dominate the structure of young disks. The results are compared to observations of local galaxies in an attempt to understand the origin of thick disks. We consider the likely contraction of the original thick disk if the thin disk accretes at a later time. We also compare the observations to the predictions of numerical simulations.

2. Data

The Hubble archival UDF images made with 4 filters were used for this study (observed and processed by S. Beckwith and coworkers in 2004). They include: F435W (B band, hereafter B_{435}; 134880 s exposure), F606W (V band, V_{606}; 135320 s), F775W (i band, i_{775}; 347110 s), and F850LP (z band, z_{850}; 346620 s). The images are 10500 x 10500 pixels with a scale of 0.03 arcsec per px.

The chain and edge-on spiral galaxies studied here were selected from our UDF catalog (EERS), which included 884 galaxies classified into 6 morphological types: chain, double, tadpole, clump cluster, spiral, and elliptical galaxies. There are 114 chain galaxies and 269 spiral galaxies in the catalog. To select edge-on spirals, we began with the 37 that have an axial ratio less than 0.3, as determined by ellipticity fits in IRAF. Of these, 32 were selected for measurement here because they avoid bright stars and neighboring galaxies. The results from these 32 will be given below. A more refined subsample of 14 edge-on spirals was considered to include the best cases on the basis of brightness, size and apparent low inclination; they will be discussed separately as the "best-case" sample. Figure 1 shows 6 examples of these best spiral cases viewed in the i_{775} band. For the chain galaxies, we selected 80 good cases that are relatively isolated in the UDF, and a best-case subsample of 34 that are bright and well resolved. Figure 2 shows 6 chain galaxies from these best cases at i_{775} band.

Major and minor axis intensity profiles in each filter were made using the task *pvector* in the Image Reduction and Analysis Facility (IRAF[1]). This task gives the intensity along

[1]IRAF is distributed by the National Optical Astronomy Observatories, which are operated by the Association of Universities for Research in Astronomy, Inc., under cooperative agreement with the National Science Foundation.

a line, averaged over the width of the line. The major axis profile was several pixels wide to include the whole galaxy. For the chain galaxies, the minor axis cut had a width equal to the length of the major axis, again to include all the light. For the spiral galaxies, two perpendicular cuts were made, one on each side of the bulge. In the discussion below, only the average of these two spiral profiles will be considered, although both were viewed to look for possible contamination by excessive noise, bright stars, and other galaxies; when contamination was present, only one side was used.

Scans and Gaussian fits were also made in four passbands for 15 unsaturated stars in the UDF images. The average Gaussian sigma values were found to be 3.01 px, 3.07 px, 3.02 px, and 3.46 px in B_{435}, V_{606}, i_{775}, and z_{850} filters, respectively. In what follows, these are taken to be the sigma of the point spread functions, used to deconvolve the instrument response from the observed galaxy scans.

3. Analysis

3.1. Scale Heights

We are interested in the intrinsic widths and lengths of the UDF galaxies for comparison with the sizes of disk components in modern galaxies. To measure these quantities in the UDF, we fitted the perpendicular *pvector* scans to convolutions of the star profiles with certain intrinsic functions, such as exponential and sech^2. The sech^2 function is the equilibrium distribution of density perpendicular to an infinite isothermal layer; it is asymptotically exponential at large distance and Gaussian at small distance. The fit was done by varying the center, width, and amplitude of the intrinsic function in nested iteration loops, convolving this function with the star profile, and then finding the values of the center, width and amplitude that gave a minimum rms difference between the convolved profile and the observed scan.

Figure 3 shows as a solid line (red in electronic edition) the perpendicular scan for the chain galaxy UDF 7037, which was illustrated in Figure 2. The star profile is the narrow (green) line. Two intrinsic functions are illustrated, an exponential in the top panel and a sech^2 in the bottom panel. The best fit intrinsic functions are shown by dotted curves and the fits themselves, which are the convolutions of the intrinsic functions with the star profile, are shown as solid curves (blue). The vertical scale is linear on the left and logarithmic on the right. Both exponential and sech^2 functions are good fits in the outer parts (out to the image noise), but the exponential function is not a good fit in the inner part because it is too peaked. In what follows, we use the sech^2 function to characterize the perpendicular profiles

of the chain and spiral disks. The resultant scale height is denoted by z_0 in the expression $\mathrm{sech}^2(z/z_0) = 4/\left(\exp\left[z/z_0\right] + \exp\left[-z/z_0\right]\right)^2$.

The relationship between the sech^2 scale height and the exponential scale height in a fit of vertical light distribution depends on how far the scan goes into the halo. If the scan follows the light far into the halo, then the halo region where the profile is intrinsically exponential dominates the fitted height and the exponential model gives a value for the height that equals half the value of the sech^2 model. If the scan extends to only one or two scale heights before it is lost in the noise, then the two models give more similar values for the height. Usually galaxy scans include large vertical distances and the factor of 2 applies; this is the case here as well. Then the Milky Way would have a value of sech^2 scale height, z_0, in the range from 1.2 kpc to 1.8 kpc (see Sect. I).

Figure 4 shows the major axis profile of the chain galaxy UDF 7037, made from a scan 17 pixels wide. The profile is not exponential and is dominated by the large clumps visible in the image in Figure 2. This type of profile is typical for chain galaxies. Spiral galaxies have smoother major axis profiles with a central bulge. Other examples of spiral and chain galaxy profiles are in Elmegreen, et al. (2004a) and Elmegreen et al. (2005b, hereafter EEVFF).

Figure 5 illustrates the quality of the scale height fits for each galaxy. The plus symbols are spirals and the dots are chains. For each, the large symbols are the best cases and the small symbols are all of the others in the selected UDF sample. The abscissa is the perpendicular scale height in pixels and the ordinate is the ratio of the rms deviation between the fit and the data divided by the peak value of the intensity scan. These ratios tend to be slightly smaller for the thicker galaxies, and slightly smaller also for the best cases, indicating better signal to noise ratios. Most ratios cluster around 5%, which we consider to be a measure of the average fitting accuracy for both spirals and chains. The B_{435}-band has more galaxies with relative rms values exceeding 0.1 than the other bands because the galaxies are often faint in B as a result of their high redshift. The minimum scale height that can be fitted is ~ 2 pixels.

The relative error in the fitted scale height was determined by comparing the best fit height, z_{0i} for galaxy i, with the height that has a relative rms fit different from the best-fit solution by 10%, z'_{0i}. In both cases the scan centers and amplitudes were fitted before this height comparison was made. The relative mean square of the heights around the best fit heights are given by $(1/N)\,\Sigma_{i=1}^{N}\left(z_{0i} - z'_{0i}\right)^2/z_{0i}^2$ for summation over N galaxies. The square root of this sum is the relative rms deviation of the height for a 10% deviation in the relative rms of the fit. We considered only galaxies that have relative rms fits less than 0.1, to avoid drop-out cases and other poor quality fits. The result indicated that for a relative rms fit deviation of 0.1, the relative rms height deviation was 0.15 ± 0.01 in all passbands. For a

relative rms fit deviation of 0.2, the relative rms height deviation was 0.21 ± 0.03. Considering the vertical scatter in Figure 5, which is $\sim 20\%$ of the mean value of $\sim 5\%$, the rms height is considered to be accurate to this latter deviation of $\sim 20\%$.

Figure 6 shows the distribution function for fitted scale heights measured in pixels (bottom panels) and kiloparsecs (top panels) on the z_{850} images. The conversion from pixels to kpc was done using photometric redshifts in Coe et al. (2006) and Elmegreen et al. (2006). These redshifts have an uncertainty of $0.04(1+z)$, but this uncertainty does not affect the kpc conversion much because the conversion factor is insensitive to redshift over the redshift range of these galaxies. The samples are again divided into all of the acceptable cases and the best cases. There is little difference in the mean results for the average and best-case galaxies. The mean z_{850} scale heights for spiral and chain galaxies are about the same, 4 ± 2 px and 1.0 ± 0.4 kpc for each. More precisely, the scale heights for the best case chains and spirals are 0.88 ± 0.25 kpc and 1.08 ± 0.35 kpc, respectively, and the scale heights for all chains and spirals are 0.96 ± 0.47 and 1.07 ± 0.30 kpc, respectively. The mean spiral scale height is $\sim 10\%$ larger than the mean chain scale height, but this result is statistically uncertain.

Figure 7 shows the redshift distributions of scale height in kpc on the z_{850} images. Large symbols again denote the best-case sample. The scale height does not change noticeably with redshift, although the lowest redshift spiral and the two lowest redshift chains, both of which are in the best-case samples, have relatively small scale heights. Perhaps we are viewing the beginning of the thin disk phase by this late epoch (or the anomaly could be just a fluke of low number statistics).

3.2. Color Gradients

The scale heights in the four passbands were compared to see if there is a vertical color gradient. Generally the disks were found to get slightly redder with height. Because the B_{435} image is often faint and sometimes even blank for the high redshift cases (the drop-outs), we make this comparison in Figure 8 using the V_{606} and z_{850} bands. The plotted quantity is the $V_{606} - z_{850}$ color fitted to one z_{850}-band scale height off the midplane minus the $V_{606} - z_{850}$ color fitted to the midplane. For a sech^2 function, this color excess comes from the expression

$$\Delta\left(V_{606} - z_{850}\right) = -5 \log\left(\frac{e^1 + e^{-1}}{e^{z_{0,Z}/z_{0,V}} + e^{-z_{0,Z}/z_{0,V}}}\right). \quad (1)$$

The figure shows reddening typically between 0.1 and 0.7, with a peak in the distribution for the best-case chains at 0.4 mag, and a peak in the distribution for the best-case spirals

at 0.3 mag. The statistical significance of the 0.1 mag difference between these two peak color excesses is low. The important point is that the midplanes are several tenths of a magnitude bluer than the high latitude emissions. Because only the ratio of scale heights for each galaxy determines this result, it is independent of redshift.

3.3. Colors and Ages

Restframe colors were found for as many galaxies as possible by interpolating magnitudes between the observed passbands and using the photometric redshifts, which have uncertainties of approximately $0.04(1 + z)$. These redshift uncertainties correspond to an uncertainty of approximately ± 0.15 in $B_{435}-V_{606}$ color, which is about the same as the photometric uncertainty in the color. We are interested in the colors at the midplanes and at one scale height from the midplane using the model fits, so we cannot use NICMOS photometry as the angular resolution of NICMOS is too poor to resolve the edge-on disk. Thus we are limited to the galaxies with $z < 0.40$ for restframe $B_{435}-V_{606}$ colors. There are 4 galaxies with such low redshifts, UDF 4907, C2 (from EERS), UDF 3974, and UDF 5454. Their midplane restframe $B_{435}-V_{606}$ colors are -0.1, 0.33, 0.71, and 0.35 mag, and their $B_{435}-V_{606}$ color gradients from the midplane to one scale height at z_{850} are -0.16, 0.28, 0.82, and 0.04 mag, respectively. The errors in these measurements can be assessed from the ratios of the rms deviations around the fitted sech^2 functions to the observed peaks (Fig. 5). The averages of the ratios for the B_{435} and V_{606} passbands for these 4 galaxies are 12%, 8%, 11%, and 5%. The most accurate values are for galaxies C2 and UDF 5454, which give restframe $B_{435}-V_{606} \sim 0.34$ in the midplane. This color corresponds to a population age of ~ 0.7 Gy for either an initial burst of star formation or an exponentially decaying star formation rate with a relatively short timescale ($< 10^8$ yrs). For a decay time of $10^{8.5}$ yrs or 10^9 yrs, the age is 1 or 1.9 Gy, respectively. These conversions from ACS colors to age were done using the spectra in Bruzual & Charlot (2003) with the Chabrier (2003) IMF and the appropriate ACS filters, as described further below.

We also determined $B_{435}-V_{606}$ and $V_{606}-z_{850}$ colors in the midplane and at one z_{850}-band scale height for all of our galaxies, and compared them with redshifted colors calculated from population synthesis models. Figure 9 shows the distribution of the observed colors with redshift. The filled circles and squares are the best cases. The dots and filled circles are for the midplane values and plus symbols and filled squares are for the off-plane positions. The rising color at high redshift results from redshifting of the Lyman continuum limit. There is little vertical color gradient in $B_{435}-V_{606}$ so the symbols overlap in the lower panels. The $V_{606}-z_{850}$ gradient mentioned above is evident in the displacement between the midplane

and off-plane values in the top panels.

To determine population ages, we reproduce the $B_{435}-V_{606}$, $V_{606}-i_{606}$ and $i_{775}-z_{850}$ color evolution models from EE05. These models considered a Chabrier (2003) IMF in the low resolution Bruzual & Charlot (2003) spectral tables with $Z = 0.008$ (0.4 times the solar abundance). They included exponentially declining star formation rates with various decay times starting at $z = 6$. To determine the colors, the population synthesis spectra were redshifted to certain z values, integrated over time using the star formation rate as a weighting factor, diminished by absorption from Hα lines (Madau 1995) and dust (Rowan-Robinson 2003; Calzetti et al. 2000; Leitherer et al. 2002), and then integrated over the ACS filter functions to get the intensity in each filter per unit solar mass of stars. The ratios of intensities in different passbands give the colors. The results do not differ significantly for $Z = 0.004$.

The models are shown in Figure 9 with solid lines for a duration of star formation equal to 1 Gy and dashed lines for a duration of 0.5 Gy. The star formation decay times are 0.1 Gy (red curves in electronic version), 0.3 Gy (green), 1 Gy (blue), and infinity (continuous star formation, black curves), increasing as the models get bluer. The midplane data points lie close to the curves with long decay times, indicating there is still a lot of active star formation in the midplane. This is true for all redshifts and colors. The off-plane $V_{606}-z_{850}$ colors in the top panels imply decay times that are shorter than the ages, 0.1 Gy for an age of 0.5 Gy, and 0.3 Gy for an age of 1 Gy. The lack of a color gradient in $B_{435}-V_{606}$ could be a result of the closeness of the contours for different decay times.

We conclude that the edge-on disks in the UDF are relatively young, with dominant stellar luminosity ages in the range from 0.5 Gy to 1 Gy. There is still significant star formation at all heights, with slightly more recent star formation in the midplane. There could be older, fainter stars in these disks as well, so we cannot get the absolute disk ages from the optical images. At these redshifts, we see mostly the uv light from young stars in the galaxy restframes.

For comparison, Yoachim & Dalcanton (2006) got a mean thick-disk color of B-R$\sim$ 1.4 for nearby galaxies. This corresponds to an age of 10 Gy for the Bruzual & Charlot (2003) models with either $Z = 0.008$ or 0.004. Gilmore, Wyse & Jones (1995) suggested the Milky Way thick disk is 12 Gy old. These ages are consistent with the young ages we see in the UDF where the look-back time is 5-12 Gy.

3.4. Surface Brightnesses

The distributions of restframe B_{435} and V_{606}-band surface brightnesses at the midplanes of the galaxies are shown in the bottom panels of Figure 10 (solid and dashed lines, respectively). These come from the sech^2 fits to the whole perpendicular profiles and not the brightness values of the central pixels (which are blurred by the point spread function and slightly noisy). There are many more B_{435} values than V_{606} values plotted because the redshift limits required for interpolation between the HST bands are $z < 0.95$ and $z < 0.40$ respectively, and there are few galaxies at low enough redshift to interpolate into the V_{606} band. The surface brightness levels are dimmed by cosmological expansion, so the intensities are corrected in the top panels to rest-frame intensities by multiplying by $(1+z)^4$. The restframe corrected midplane surface brightness for chains ranges from 19.5 to 25 mag arcsec^{-2} in B_{435} and from 22.5 to 24.5 mag arcsec^{-2} in V_{606}. The range for spirals is 21 to 25 mag arcsec^{-2} in B_{435} and $\sim$ 24.75 mag arcsec^{-2} in V_{606}. These are apparent surface brightnesses, which means edge-on through the disks of these galaxies. Although the average restframe B_{435} surface brightness is brighter than the average restframe V_{606} surface brightness for this sample, three of the four low-redshift galaxies that give restframe V_{606} surface brightnesses (all chain galaxies) have fainter B_{606} magnitudes, and therefore red colors, as discussed above.

There is a slight correlation between restframe B_{435} surface brightness and scale height in the z_{950} band, as shown in Figure 11. The thicker and generally larger galaxies have brighter midplane surface brightnesses. These are edge-on galaxies, so this correlation is sensible if the midplane surface brightness is the midplane stellar density multiplied by the path length through the disk. The midplane extinction appears to be lower than in modern disk galaxies, as suggested by the reddening with height, so the path length through the midplane is larger for larger galaxies. We show below that galaxies with larger scale heights also have larger diameters.

The observed surface brightness in the z_{850} band is shown versus redshift in Figure 12. The dimming with redshift is slower than the cosmological intensity factor of $(1+z)^{-4}$, shown by the curved line. Chains and spirals have about the same distribution, but the low redshift spirals are brighter than the low redshift chains. Histograms of these distributions, compressed along the redshift axis, were shown in Figure 10.

3.5. Mass Column Densities

We converted the apparent z_{850}-band surface brightness (Fig. 12) into mass surface density by assuming an age and star formation decay time of 1 Gy, as estimated above from Figure 9. We used the ACS filters with the Chabrier (2003) IMF and the Bruzual & Charlot (2003) spectral tables for $Z = 0.008$. Galactic dust and intervening hydrogen absorption were included (see above).

For an apparent z_{850}-band surface brightness of 24 mag arcsec^{-2} and a redshift of 1 (Fig. 12), the mass column density measured edge-on through a disk is 24 $M_\odot$ pc^{-2} with 1 Gy age and decay timescales. For a surface brightness of 25 mag arcsec^{-2} at $z = 3$ (also from Fig. 12), the mass column density is 125 $M_\odot$ pc^{-2} with these times. With continuous star formation instead of an exponential decay time of 1 Gy, these column densities become 18 and 78 $M_\odot$ pc^{-2}, respectively. For continuous star formation with an age of 0.5 Gy, they become 12 and 43 $M_\odot$ pc^{-2}.

The mass column density perpendicular to the plane may be estimated from the edge-on value divided by the length-to-width ratio of ~ 3, given in Section 3.7 below. These perpendicular values depend on redshift and age assumptions, but are in a range from 4 to 40 $M_\odot$ pc^{-2}. For spiral galaxies at $z \sim 1$, where the average apparent z_{850} surface brightness ranges between ~ 23.5 and 25 mag arcsec^{-2} and the ratio of axes is ~ 2.3 (see below), the mass column density for 1 Gy age and 1Gy decay time ranges between 4 and 16 $M_\odot$ pc^{-2}.

The surface density of the thick disk in the Milky Way solar neighborhood may be estimated from the surface density of the old thin disk (~ 70 $M_\odot$ pc^{-2}; Freeman 1987), the density ratio of the thick to the thin disk, which is $\sim 5\%$ (Robin et al. 1996; Buser et al. 1998; Ojha 2001; Kerber et al. 2001; Chen et al. 2001; Du et al. 2003) to 13% (Chen et al. 2001; Seigel et al. 2002), and the scale height ratio of the thick to the thin disk, which is ~ 2 in these references. The product, $\sim 7 - 15$ $M_\odot$ pc^{-2}, is the thick disk mass column density perpendicular to the local Milky Way plane. This value is within the range of values found here for the thick disks of UDF galaxies.

3.6. Distribution of Vertical Clump Positions and Sizes in Chain Galaxies

Spiral and chain galaxies are very clumpy in the UDF, as indicated by the images in Figures 1 and 2. The chains are probably edge-on versions of clump-cluster galaxies, which were discussed in more detail elsewhere (EEH04; EE05). The relative emission from giant clumps in all of the UDF clump cluster galaxies is 0.27 ± 0.14 (EEVFF). For the spirals, it is 0.08 ± 0.065, not counting the bulges (EEVFF). The spiral clumps are similar in magnitude

and color to the chain and clump-cluster clumps (EEH04; EE05), so spirals differ by having a more prominent interclump emission (in addition to bulges and exponential disk profiles).

We have proposed that galaxy disks evolve along a sequence of decreasing clump prominence, from clump clusters, chains, and clumpy spirals at high redshift to normal spirals today (EEVFF). Some of the clumps in clump cluster and chain galaxies may move to the nucleus and form a bulge, as suggested by numerical simulations in Noguchi (1999) and Immeli et al. (2004a,b), but we see no direct evidence for this and believe it is more likely that the clumps dissolve where they are. This conclusion comes from the similarity between internal clump densities and background galaxy tidal densities, from the appearance in some cases of tails associated with the clumps, and from the relatively low mass fraction of the clumps (EE05). The density similarity implies the clumps are eventually dispersed by in-plane tidal forces. We also noted the similarity between the radial distribution of the average clump luminosity in UDF clump cluster galaxies and the exponential distribution of UDF spiral disks. All of these results suggest that the giant clumps in clump cluster and chain galaxies dissolve more-or-less in place and merge to form a smooth exponential disk.

The edge-on galaxies in the present study allow us to study the implications of clump dissolution on the vertical profiles of galaxy disks. We did this in two ways. First, the intensity profiles of all of the prominent clumps in the 6 best-case chain galaxies in Figure 2 were measured in strips 3 pixels wide. These scans were also fitted to sech^2 functions, using the same star profile deconvolution technique as for the disks. The resultant clump scale heights are shown as crosses in Figure 13, along with the scale heights for the disks, which are shown as solid lines. The abscissa is the passband and the ordinate is the height in kpc. For each galaxy and passband, a different cross is plotted for each different clump. Interclump regions were also scanned, and their fitted scale heights are shown as circles in Figure 13. The heights for clumps and interclump regions in three of the spiral galaxies of Figure 1 are shown in Figure 14.

Figures 13 and 14 show again the tendency for the disks to redden with height, as the scale heights increase with wavelength. The same is true for clumps. The figure also indicates that the clump scale height is $\sim 80\%$ of the disk scale height. This near agreement of disk and clump scale heights is not too surprising considering that the disk profile has a substantial contribution from the clumps. Nevertheless, the clumps are about as thick as the whole disks. The clump diameter of 1-2 kpc is only slightly smaller than the in-plane clump diameter, measured to be 1.8 kpc for a sample of 10 clump cluster galaxies in the UDF (EE05). The interclump regions are generally thicker than the clumps for both chains and spirals, and comparable to the whole disks.

Secondly, to study vertical clump properties we measured the clump centroid positions

for each chain galaxy in our UDF catalog to one pixel accuracy. These positions were then fitted to a line for each chain galaxy (the midplane line) and the perpendicular distance between each clump centroid and the line was determined. The rms deviations of these perpendicular distances were calculated for each chain galaxy. Figure 15 shows the distribution function of the rms deviations in pixels (bottom panel) and kpc (top panel). Both panels have their histograms plotted on linear scales, but in the top panel, we also plot the kpc distribution on a log-linear scale using a solid line; the corresponding log scale is on the right. The clumps in chain galaxies typically deviate from the midplane by 0.4 pixel on average, which corresponds to ~ 100 pc when the individual redshifts are applied. This is an upper limit to the physical deviation because the measuring accuracy is only one pixel. Such a small deviation compared to the clump scale height is consistent with our visual impression that chain galaxies are fairly straight. The solid line at the top of Figure 15 is nearly straight, indicating that the distribution of clump centroids and their measurement errors combined is approximately an exponential function of distance from the midplane with a scale height of ~ 85 pc.

The confinement of clumps to the midplane seems to imply that they formed there rather than came in from outside. If they are accreted satellites, then they have to settle to the midplane before they dissolve. In situ formation suggests gravitational instabilities are involved. We discuss this more in Section 4.1.

3.7. Radial Scale Lengths

The parallel *pvector* scans for each edge-on spiral galaxy were fitted to projected exponential functions to find the radial scale lengths. A projected exponential intensity function $I(x)$ for projected distance x in a disk with unit scale length and maximum radius r_{max} is $I(x) = 2\int_0^{y'(x)} e^{-r} dy$ for $r^2 = x^2 + y^2$ and $y'(x) = (r_{max}^2 - x^2)^{1/2}$. Again the fitting procedure iterated over center position, scale length and peak intensity, finding the minimum rms deviation between the observed profile and the convolution of the intrinsic function and the star profile. The radial scale lengths for spiral galaxies in the UDF were studied in more detail elsewhere (EEVFF). They are smaller than radial scale lengths in modern galaxies, and this result, combined with the fact that the UDF spirals have density waves, suggested that these galaxies grow from the inside out (EEVFF; see also Papovich et al. 2005). Here we are primarily interested in the ratio of the radial to the vertical scale length. The radial scale lengths alone are not as dependable for edge-on spirals as they were for face-on spirals in our previous study because for edge-on spirals there is a possibility of midplane extinction (even though the midplanes are relatively blue for our galaxies – see Fig. 8).

We also attempted to fit the parallel profiles of chain galaxies with projected exponential functions, but the intrinsic profiles are clearly not exponential in most cases (Elmegreen, et al. 2004a; EEVFF) so the resultant scale lengths were sensible for only a few chains. Instead, we measured the chain galaxy lengths directly, from the center of the clump at one end to the center of the clump on the other end.

Figure 16 shows the radial scale lengths of the spiral galaxies in the right-hand panel and half the end-to-end lengths of the chains in the left-hand panel, all for the z_{850} band. The bottom panels plot these lengths versus the redshift, showing a slight increase in the largest galaxy size with decreasing redshift. The top panels plot the vertical scale heights versus the radial lengths. The scale height increases slightly for larger galaxies.

The distribution function of the ratio of the z_{850}-band radial scale length, or half-length in the case of chains, to the height is shown in Figure 17. The solid histograms are for the best cases, and the dashed histograms are for all the galaxies. The mean ratio of radial scale length to perpendicular scale height for the best-case spirals is 2.3 ± 0.7, and the mean ratio of the half-length to the height for best-case chains is 3.4 ± 1.6.

These ratios are consistent with our previous results based on the distributions of axial ratios. For example, the distribution of width-to-length ratios, W/L, was determined for 269 spirals in the UDF based on outer isophotal contours at 2-σ above the image noise (EERS). This distribution decreases at small W/L with a half-maximum position in the decrease occurring at $W/L = 0.3$ (Fig. 8 in EERS). For local spirals of Types 3 to 8 in the Third Reference Catalogue of Bright Galaxies (de Vaucouleurs et al. 1991), this half-maximum point is at $W/L \sim 0.1$ (EERS). The W/L ratio for UDF spirals is slightly smaller than the inverse of the scale length to scale height ratio for spirals found in this paper (0.4) but here we corrected for projection effects. If we fit the observed intensity profile along the major axes of our spirals by an exponential function, rather than a projected exponential function, then the average ratio of scale length to scale height would be 3.1 ± 1.1. The inverse of this is more in line with the W/L ratio, which also has no projection corrections. For chains and clump-cluster galaxies combined (i.e., different orientations of the same objects), the distribution of W/L decreases at small W/L with a half-maximum position occurring at $W/L \sim 0.2$ (EE05). This W/L based on 2-σ isophotal contours is a slightly different measure than our ratio of half-length to scale height here, but the two are consistent with each other, and both indicate relatively thick disks for chain and clump-cluster galaxies.

4. Discussion

4.1. Summary and Implications of the Results

The edge-on galaxies in the UDF have disks that are 1.1 ± 0.4 kpc thick for spirals and 0.9 ± 0.3 kpc for chains. No thin disk components or dust lanes can be seen, although resolution limits would make this difficult (a pixel is typically ~ 250 pc). There is probably some thin disk component in the spirals because there are spiral density waves in the face-on versions; such waves propagate best in a disk that is thinner than the interarm spacing. There are no spirals in clump cluster galaxies, however, so if chain galaxies are the edge-on counterparts of clump-clusters, then it is possible the chains do not have thin disk components inside the observed thick disks. This difference between spirals and chains is consistent with our proposal that chain and clump-cluster galaxies are young versions of spiral galaxies (if they survive major mergers; EEVFF).

The restframe and observed colors of the galaxies suggest active star formation in the midplane and slightly less active star formation off the midplane. Color ages are in the range from 0.5 Gy to 1 Gy, with star formation rates either continuous during that time or slowly decaying. For these ages, the edge-on surface brightnesses correspond to perpendicular mass column densities between 4 and 40 $M_\odot$ pc^{-2} depending on redshift and galaxy size; for spirals it is between 4 and 16 $M_\odot$ pc^{-2}. The column density of the Milky Way thick disk in the solar neighborhood is comparable, $\sim 7 - 15$ $M_\odot$ pc^{-2}.

There is a gradual reddening of the UDF disks with height, by 0.3-0.4 mag in $V_{606}-z_{850}$ over one scale height, which is consistent with the lack of thin and prominent dust layers. This gradient corresponds to $0.3 - 0.4$ mag kpc^{-1} in restframe U-B for $z \sim 1$. Local thick disks have smaller or no reddening gradients with height. For example, Mould (2005) found a vertical gradient in V-I of $\sim 0.06 \pm 0.02$ mag kpc^{-1} for four local galaxies. Our high redshift color gradients should be larger than local color gradients for several reasons. First, the restframe U-B colors seen at high redshift by the ACS are very sensitive to stellar population age for ages less than $\sim$ 1 Gy, but the restframe V-I colors seen locally are less sensitive to ± 1 Gy formation times when the population has already aged 10 Gy. For a Bruzual & Charlot (2003) model with a Chabrier (2003) IMF and metallicity $Z = 0.008$, U-B increases by 1.0 mag as a starburst ages from 0 to 5×10^8 years. However, the increase in V-I between 9.5 Gy and 10 Gy old populations, which have the same 5×10^8 yr star formation age spread, is only 0.11 mag. Thus, young U-B color gradients in ACS galaxies should evolve into much smaller V-I color gradients in today's galaxies. A second change over time is that the stars in thick disks at high redshift should mix vertically during the intervening minor mergers. Similarly, the thick disks in major merger remnants today should be a mixture of the thick

disk and other stars from the previous galaxies.

There is no obvious trend in disk thickness with redshift, and only a slight trend in disk length with redshift. The ratio of radial scale length to disk height is 2.3 ± 0.7 for spirals. Exponential fits along radius could not be made for the chains, so we measured instead the ratio of the half-length to the disk height, which is 3.4 ± 1.6. These measurements are consistent with other observations of pervasive thick disks at high redshift. The implication is that most or all galaxy disks were thick at early times, from $z = 0.5 - 4.5$ in our sample, which corresponds to look-back times of 4.8 Gy to 12.2 Gy in the standard cosmology.

Such pervasive disk thickness is not surprising given the small mass column densities in the disks we observe (Sect. 3.5) and in the original Milky Way thick disk. Using the equilibrium relation for sech^2 scale height $z_0 = a^2/(\pi G \Sigma)$, we expect the observed $z_0 \sim 1$ kpc for a velocity dispersion of only $a = 14$ km s^{-1} when the mass column density is comparable to that of the Milky Way thick disk, $\Sigma \sim 15$ M$_\odot$ pc^{-2}. In comparison, the velocity dispersion of the Milky Way thick disk is much larger, ~ 35 km s^{-1}, because of the additional disk mass from the thin disk. These considerations suggests that most high reshift disks should be thick for star formation at normal interstellar velocity dispersions, and that local thick disks may have a qualitatively different origin (i.e., they require much more heating). We discuss this comparison more in the next section.

The UDF disks have giant clumps that are probably star-forming regions with ages of $\sim 100 - 300$ My (EE05). These clumps are centered within ± 100 pc of the midplane for our complete sample of chain galaxies. This small dimension is partly a selection effect because chains are defined to be linear objects. There are other clumpy UDF galaxies with more irregular shapes that could have intrinsically larger rms clump positions. In any case, the chains as a class appear to have rather relaxed vertical structures, and the sizes of the clumps that comprise them are only $\sim 20\%$ less than the disk scale heights. This relative flatness and the similarity in clump and disk sizes suggest that the clumps form inside the disks and then dissolve in place to form the disks. This is analogous to star formation in modern thin disks but the star cluster scale in the UDF ($0.4 - 1$ kpc in radius according to Fig. 13) is much bigger than the star cluster scale in today's galaxies. A more relevant comparison might be between modern star complexes and UDF clumps, because both are at the top of a hierarchy of young stellar structures. Star complexes in local galaxies measure $\sim 400 - 800$ pc along the plane and ~ 100 pc perpendicular to the plane (Efremov 1995). They are often separated by ~ 2 kpc along the arms of large spiral galaxies. These in-plane dimensions are comparable to the in-plane dimensions of UDF clumps, but the vertical dimensions are ~ 10 times larger in the UDF. Star complexes most likely form by gravitational instabilities in today's thin disks, with a separation and characteristic in-plane scale given by the ambient

Jeans length for a disk, $\lambda \sim 2a^2/G\Sigma$. With velocity dispersion $a \sim 10$ km s^{-1} and gas mass column density $\Sigma \sim 20$ M$_\odot$ pc^{-2}, this gives $\lambda = 2.3$ kpc for modern disks. The same in-plane separation should apply to high redshift disks but it should also apply approximately to the vertical direction at high redshift because the whole disk column density at high redshift is small, not just the gas disk column density as in modern galaxies.

4.2. More Comparisons with Modern Galaxies and a Consideration of Adiabatic Thick Disk Contraction

The thick disks at high redshift should also be compared to modern thick disks in their absolute heights and length-to-width ratios. In the largest recent survey, Yoachim & Dalcanton (2006) determined the scale heights for thick disk components of local galaxies using the same sech^2 function as that used here and found an average relation $z_0 = 1.4\left(V/100 \text{ km s}^{-1}\right)$ for circular rotation speed V. These modern values are larger than ours by a factor of ~ 1.5 on average, but the modern galaxies have larger radial sizes too. The ratio of radial exponential scale length to vertical sech^2 scale height in the Yoachim & Dalcanton sample, 3.4 ± 1.7, is about the same as ours, which is 2.3 ± 0.7 for spirals and 3.4 ± 1.6 for chains. Thus the UDF scale heights are about the same as local scale heights for similarly small galaxies. This size similarity, along with the observed young ages, suggests we are witnessing the formation of the thick disk component in young galaxies. The confinement of the star-forming clumps to the midplanes and their similarity in size to the scale heights of the thick disks suggests further that the mechanism of thick disk formation is the dissolution of giant star clusters. These clusters may form by gravitational instabilities, as illustrated by Noguchi (1999) and Immeli et al. (2004a,b) under similar conditions.

There are three problems with this simple interpretation of the observations. First, the galaxies are smaller than local galaxies, on average (EEVFF), and if they are supposed to grow by accretion into modern L* galaxies, then both their radial scale lengths and thicknesses have to grow in order to keep the ratio of axes about the same. If the Yoachim & Dalcanton (2006) scaling is applied to the Milky Way where $V \sim 220$ km s^{-1}, the vertical scale height would be $z_0 \sim 3$ kpc, meaning it has to grow by a factor of 3 from the observed 1 kpc average at high redshift. The radial scale length has to grow as well, by a factor of ~ 4.4 if the $\sim 2.3 \pm 0.7$ ratio of axes for high redshift spirals converts to a 3.4 ± 1.7 ratio for modern spirals (Yoachim & Dalcanton 2006). This mutual growth implies that if the thick disk formation process continues to be through the dissolution of massive clusters, there should be stars in modern thick disks that are fairly young, going back only to the time when the radial growth stopped, if it ever did. As thick disks appear to be mostly old today

(older than 10 Gy for the Milky Way – Gilmore, Wyse, & Jones 1995; Furhmann 1998), they could not have grown for as long a time as the thin disk.

Second, a high fraction of the galaxies we observe in the UDF could merge together or into larger galaxies over time (see merger trees in Brook et al. 2005). Any such merging would destroy the structures we observe here. However, merging would not cool a hot disk, so the thick disk stars in the present sample are likely to end up as thick disk stars in the merger remnant, or perhaps as halo stars if the merger is violent. After the last major merger, the thick disk component of the final galaxy should contain the previous thick disk components of the earlier galaxies. Such thick disks would not be simply the superposition of dissolved giant star clusters, and modern thick disks that form in this way would not be expected to resemble the high redshift thick disks that we observe here (i.e., with midplane clumps having the same size).

Third, any slow accumulation of young thin disk material inside a thick disk will pull in the thick disk because of the extra midplane gravity. Figure 18 shows a solution to the two-fluid coupled equations:

$$dP_i/dz = -g\rho_i \quad ; \quad P_i = \rho_i a_i^2 \propto \rho_i^\gamma \quad ; \quad g(z) = 4\pi G \int_0^z (\rho_0 + \rho_1)\, dz \tag{2}$$

where $i = 0$ and 1 for thin and thick disk material. The pressure equilibrium equations are separate but the gravitational forces of the two fluids are coupled (see also Jog 2005). The figure also shows the single fluid solution representing an initial pure-thick disk that has the same mass column density as the "thick disk after" solution. Both the single fluid solution ("thick disk before") and the thin+thick disk combined solution ("after") are equilibria.

To make this solution, we varied the initial thick disk scale height and the final thin disk velocity dispersion (a) until the final thick+thin disk resembled the Milky Way. We assumed that the thick disk column density remains constant at 15 $M_\odot$ pc^{-2} (see above) as the colder thin disk material is added. We assumed the final thin disk column density is 70 $M_\odot$ pc^{-2}, as in the Solar neighborhood, and the ratio of midplane densities for thick and thin disks in the final state is 8%, which is also typical for measurements locally. The thick disk velocity dispersion is allowed to increase adiabatically during its contraction with the usual three dimensional adiabatic index, $\gamma = 5/3$ (this assumes that stellar heating during the one-dimensional contraction is distributed in all three dimensions). The velocity dispersion of the cold component is assumed to be constant, and fitted to 18.5 km s^{-1} to give the desired final state. The other variable was the initial thick disk scale height, from which the initial velocity dispersion follows given the assumed thick disk mass column density. This initial height was found to be 3 kpc for the best final-state fit, giving an initial velocity dispersion of 25 km s^{-1} for the assumed mass column density.

These solutions suggest that an initial thick disk of 15 $M_\odot$ pc^{-2}, with a sech^2 scale height of 3 kpc and a 25 km s^{-1} velocity dispersion, can contract to a final disk component representing 8% of the midplane density with a $1/e$ height (not sech^2 height) of 875 pc and a velocity dispersion of 38 km s^{-1} when a thin disk component is slowly added, where the thin disk has a final $1/e$ height of 350 pc and a velocity dispersion of 18.5 km s^{-2}. These numbers for the final state resemble the thin and thick disk of the local Milky Way. The problem is that the initial pure-thick disk in the model has a sech^2 height of 3 kpc, which is much larger than we observe in the UDF (where the average is 1.0 kpc).

Gnedin et al. (2004) considered a similar problem of halo contraction during disk build-up for a Milky Way model. They found that the density of the halo increases by a factor of ~ 5 within ~ 1 kpc of the galactic center and that this increase is comparable to that obtained in a simple adiabatic model. Figure 18 has a similar density increase in the central part of the thick disk.

To turn the problem around, we considered what would happen to an observed 1 kpc thick disk with a mass column density of 15 $M_\odot$ pc^{-2} when a 70 $M_\odot$ pc^{-2}, cold (~ 20 km s^{-2}) thin disk accretes through it. The new equilibrium would have the original thick disk contract to a scale height that is the same as the final thin disk scale height, ~ 350 pc, and the resulting velocity dispersion for both would be ~ 20 km s^{-2}. They would appear as a single component with a small fraction of very old stars in addition to the young thin-disk stars (old thin disk stars were also found in simulations by Abadi et al. 2003 for a different reason). Unless the thin disk mass is already present inside the UDF galaxies, the thick disks we are seeing in the UDF are probably not the precursors of today's thick disks, even though they look about the same as today's thick disks. They could be precursors of the old thin disk component of today's disks, mixed in with whatever material accreted in the intervening time.

The model shown in Figure 18 suggests that if today's thick disk component of the Milky Way started as an equilibrium pure-thick disk at a young age, and if subsequent disk accretion was gentle (adiabatic), then the initial thick disk scale height had to be ~ 3 kpc, much larger than we observe in the UDF. The surface brightness of this component would be lower than what we see by the ratio of heights (for a fixed mass column density), which is $1/3 = 0.3$. This corresponds to a lower surface brightness by 1.3 mag. The surface brightness can be even fainter if the original thick disk was older than the disks observed here. Perhaps such ultra-thick components are present and we cannot see them. They would have an axial ratio of unity so they are more like spheroids, not disks. It is possible that early disk galaxies had both thick disks and spheroids ~ 3 times higher, and that accretion over a Hubble time brought in the original spheroid components to become modern thick disks, as it brought

in the original thick disks to become the modern old thin disks, blending them with the accreted gas and stars over time. This all assumes adiabatic gas accretion, however, and no disk stirring by satellites that might bring in the gas. It also assumes today's halo stars came in relatively late on satellites.

An alternative model is that the galaxies we observe in the UDF are not going to accrete or grow much over time, but will remain small galaxies with the observed disks becoming today's thick disk components. There would have to be relatively little thin disk accretion. This solution is plausible for these small UDF galaxies because modern galaxies of this size, the dwarf Irregulars and spheroidals, tend to have thin disk components with low surface densities (see Fig. 22 in Yoachim & Dalcanton 2006). Then we would conclude that the UDF does not contain enough galaxies to sample out far enough in the galaxy luminosity function to produce an L^* galaxy, but is mostly composed of common dwarfs. A possible problem with this interpretation is that the spirals in the UDF have strong spiral arms, whereas dwarf galaxies today do not. This implies that the ratio of visible disk mass to halo mass is larger in the UDF spirals than in today's dwarfs, and makes it unlikely that the UDF spirals will turn into today's small galaxies (EELS).

These considerations of shrinking disks do not apply if the thick disk components of modern galaxies have been heated steadily over time, either by satellite stirring or satellite debris deposition. What would change in equations 2 is the scaling of the velocity dispersion with density, which was assumed to be adiabatic. Any disk thickness can result if there is enough stirring. A problem with this continuous stirring model arises if today's thick disks are mostly old stars. Stirring without any deposition or triggering of young, high-velocity stars would seem to be difficult. If the stirring stopped at the time given by the ages of the youngest thick-disk stars, and subsequent accretion was adiabatic thereafter, then the shrinking argument applies again for subsequent times. This would seem to be the case in the Milky Way models reviewed by Freeman & Bland-Hawthorn (2002), who suggest that the Milky Way thin disk grew quiescently after $z \sim 1$. In that case, the youngest thick-disk stars would be ~ 8 Gy old. Quiescent growth by a significant mass factor would still shrink the original thick disk though.

Smooth disk accretion is favored by the observed confinement of the giant clumps, particularly in the chain galaxies, to the galaxy midplanes (Sect. 3.6). In this case the clumps most likely formed by gravitational instabilities in the disk gas (as opposed to whole clump accretion from outside). Smooth gas accretion is considered in galaxy formation models by Murali et al. (2002), Westera et al. (2002), Sommer-Larsen, Götz, & Portinari (2003), and Keres et al. (2004).

In the Introduction, we reviewed the main models for the formation of thick disks. There

are elements of all of these models in our observations of the UDF and in the analogous observations of modern thick disks: (1) Stochastic heating is likely for young stars at low velocity dispersion, particularly with giant star-forming clumps like those in the UDF as scattering centers. (2) Sudden heating during impacts from small galaxies is not observed directly in the present sample of galaxies, but it is likely to have happened at $z \geq 1$, as collisions were probably frequent. (3) Satellite debris is not likely to be the primary origin for the thick disks in the UDF because they appear too much like dissolved giant clumps. However, if the UDF thick disks shrink down during a later phase of thin disk accretion, then a new, late-stage formation mechanism would be required to form modern thick disks. This later mechanism could be the accumulation of satellite debris, particularly as the remnant streams are apparently observed in the Milky Way (e.g., Wyse et al. 2006) and there should have been many residual satellites. A counter-rotating thick disk supports this possibility too (Yoachim & Dalcanton 2005).

(4) Thick disk formation during a highly turbulent phase, before the accreted material cools to form a thin disk, is essentially what we observe in the UDF. High turbulent speeds can produce the observed giant clumps by gravitational instabilities. We note, however, that if the thick disk column density is comparable to that in the Milky Way and typical for our observations, namely $\Sigma \sim 15$ M$_\odot$ pc^{-2}, then a velocity dispersion of only $a = 14$ km s^{-1} is enough to produce a thick disk with the observed UDF sech^2 height of $z_0 = 1$ kpc (from the equilibrium equation $a^2 = \pi G \Sigma z_0$). Young disks should always be relatively thick before a significant column accumulates. In addition, the impact heating of disk gas and high accretion velocities for new gas can maintain some excess turbulence over that produced internally by supernovae and stellar winds. When the accretion rate and star formation rate decrease and this excess turbulence subsides, and when the disk mass increases, then the following generations of young stars should form a thinner disk.

Finally, (5) the thick disks in the UDF appear most directly to have formed by the dissolution of massive star clusters. The difference between this interpretation and the model by Kroupa (2002) is that the star clusters in the UDF have very large radii, rather than large velocity dispersions with radii that are small, like those of today's clusters.

We also note that the earliest interpretation of the modern thick disks as inner compressed parts of old stellar halos (van der Kruit & Searle 1981a,b), could be possible too, as discussed above.

Several questions are raised by the UDF observations. Is there a component of the old thin disk in the Milky Way and other spiral galaxies that is the compressed remnant of a thick disk that was in place at $z \geq 1$? Is there a range of ages in the thick disks of modern galaxies that suggests they grew for some extended time along with the thin disk as part

of an inside-out formation scenario? Are the ages of thick disk stars younger in the outer parts of galaxies (which formed last)? Was the accretion onto disks at early times mostly in the form of gas (rather than stars or stellar satellites) so that young stars formed *in situ* by the usual processes (i.e., midplane gravitational instabilities)? Could the modern thick disk component have been a yet-undetected spheroidal component at high redshift, compressed into a flatter form by the subsequent accretion of thin disk mass? All of these questions are within the realm of modern telescopes and numerical simulations.

4.3. Comparisons with Numerical Simulations of Thick Disk Formation

Disk galaxy simulations show many of the features reported here, but there some notable differences too. Here we review several of the recent thick disk models.

Abadi et al. (2003) found in simulations of Milky Way type galaxies that the thick disks are composed mostly ($> 50\%$) of stars brought in by satellites; among the oldest thick-disk stars (> 10 Gy), 90% are from satellites. They also found that the thin disk forms more quiescently after the last significant merger is over by converting the previously accreted satellite gas into stars. These simulations are consistent with our general results, but they do not discuss the attributes of the disks at early epochs, when we observe them here. Thus, we cannot directly compare our results to theirs.

Models by Brook et al. (2004) form thick disks from gas-rich building blocks that are accreted during hierarchical merging. The gas forms stars while it cools into a disk. This differs from the Abadi et al. model in which most of the thick disk stars formed in satellites before they accreted. Brook et al. (2004) showed images of the model during the epoch of thick disk formation ~ 8 Gy ago. The models look very clumpy, like clump cluster galaxies, but the clumps do not settle into a thick disk until rather late, 8.3 Gy ago ($z \sim 1.2$) for the model they show. We suspect that real clump cluster galaxies are more disk-like even at higher redshift, based on the distribution of the ratio of axes (EERS) and the continuation of this morphology out to $z \sim 5$ (Elmegreen et al. 2006). We also find here that the rms dispersion of the clump positions around the midplanes of the chain galaxies are immeasurably small, unlike the model in Brook et al. (2004). Thus our conclusion about the origin of these clumps, i.e. that they arise from in-plane instabilities, differs from the model in Brook et al, where they are directly accreted from outside. If clumpy accretion models eventually show more disk settling before the clumps dissolve, then an accretion origin might be able to explain the highly aligned morphology of the chain galaxy clumps. Brook et al. (2004) also find, as in Abadi et al., that the epoch of the last major merger determines the age of thick disk.

Brook et al. (2005) consider the thick disk component of their models in more detail. They see no vertical color gradient after the thick disk has evolved to the present time. As mentioned in Section 4.1, this color uniformity is consistent with the strong vertical gradient that we do see in the restframe U-B color when the thick disks are young because evolution and bandshifting remove any such gradient over time. However, the Brook et al. result is also consistent with no vertical gradient for a young age because of vertical mixing. Thus the lack of a vertical color gradient in the present-day Brook et al. models is inconclusive. It would be interesting to know the model color gradients at $z \sim 1-5$ where the chain galaxies in our survey are located. There should be a vertical gradient in the restframe U-B of ~ 0.4 mag kpc^{-1}. Such gradients would seem to be a critical test of whether thick disks at high redshift formed by mixing satellite debris (where small early gradients are expected) or by quiescent star formation at low disk surface density (where larger gradients might appear; Sect. 4.1).

The Brook et al. (2005) models have a relatively high abundance of alpha elements in the thick disk because of rapid star formation. We observe thick disk colors consistent with relatively young ages too, $\sim 0.5-1$ Gy (Fig. 9).

Further implications of the Brook et al. models are in Brook et al. (2006), who study a Milky Way-like disk after redshift $z = 1$. They find that the exponential scale length increases as redshift decreases from $z = 1$ to 0, by about a factor of 1.4, and that the vertical scale height does not change during this time. We have essentially the same result here but over a longer redshift range. We find that the z_{850}-band scale height is somewhat constant from $z = 4$ to 0 while the scale length or half-length (in the case of chains) increases a little. However the scatter in our data is too high to be conclusive about this. More to the point, though, is the change in the ratio of the length to the height for spirals in our survey. This ratio is 2.3 ± 0.7 from Figure 17, and 3.4 ± 1.7 for modern galaxies in Yoachim & Dalcanton (2006). The change is a factor of 1.5, similar to the prediction by Brook et al. (2006). There is essentially no change in this ratio for chain galaxies, but the scatter in the data is large.

Brook et al. (2006) also find that the central surface brightness of their model disk in B band at $z = 1$ is 21.0 mag arcsec^{-2}. The dimming-corrected restframe B-band surface brightness found here is fainter, 22 mag arcsec^{-2} (Fig. 10) for the edge-on spirals, and about 1 mag arcsec^{-2} fainter if we correct to a face-on view. The corrected restframe B-band surface brightness for chain galaxies is a little brighter, but still not as bright as in the Brook et al. (2006) model.

5. Summary

The transverse thicknesses of chain galaxies and edge-on spirals in the UDF were fitted to sech^2 functions and the resulting scale heights were studied as a function of redshift and galaxy size. The average scale height is 1.0 ± 0.4 kpc, with no obvious dependence on redshift. There is a $0.3 - 0.4$ mag $V_{606} - z_{850}$ color gradient over one scale height, suggesting slightly older stars at higher elevations. The midplane colors corrected for redshift or compared with redshifted stellar population models indicate star formation is still active. Luminous disk ages are $0.5 - 1$ Gy, although older stars could be present. The redshift-corrected surface brightnesses, compared with population models, suggest the mass column density perpendicular to the disk is in the range from 4 to 40 $M_\odot$ pc^{-2}, depending on galaxy size and redshift. Most of our sample is in the lower part of this range and consistent with that of the Milky Way thick disk. The ratio of axes for UDF disks is $\sim 3 \pm 1.5$, comparable to the ratio for modern thick disks.

The disks in the UDF are composed of giant clumps closely centered on the midplane. These clumps do not appear to be a swarm of satellite remnants in various stage of accretion, but appear to have formed in the disks as a result of gravitational instabilities. Their sizes are only $\sim 20\%$ less than the scale heights, which suggests the disks built up over time by the dissolution of clumps.

Modern thick disks may not be as directly related to the UDF disks as these observations suggest. If the entire disk grows over time, then it is difficult to see how the thick disk can remain old and still preserve about the same ratio of axes during growth. In addition, if thin disks form inside the thick disks observed here, as a later or continuing phase of gas accretion, for example, then the UDF thick disks should shrink down to have a size today that is comparable to the old thin disk; i.e., they would not become the thick disks of modern galaxies.

The observation of clumpy but straight thick disks in chain and spiral galaxies from redshift $z \sim 0.5$ to 5 seems inconsistent with the prevailing model in which thick disks form during the violent impact heating of thin disks and by satellite debris from this mixing. The young disks that we observe appear more quiescent, and they appear to be thick because they have low mass column densities (comparable to the mass column densities of modern thick disks, but without the underlying thin disks). If there is a phase of impact stirring to make modern thick disks out of thin disks, then it would have to come after the UDF epoch, or it would have to involve UDF morphologies (e.g., irregular collision remnants) that are not included in our spiral and chain samples.

The possibility of a selection effect like this is important to acknowledge. The whole no-

tion of chain galaxies as edge-on clumpy disks could be wrong, for example, even though the supposed face-on counterparts are observed and in the right proportion for inclination effects. Still, the galaxy sample used for study in this paper was chosen according to morphology with the thinnest members of each class used to represent the edge-on cases. If these thin galaxies are only the more relaxed members of a larger set of galaxies whose thicker vertical extents are determined by violent collisions and not face-on inclinations, then our sample would be biased. Such a bias would affect our conclusion that UDF thick disks formed by the dissolution of giant clusters which, in turn, formed by in-plane gravitational instabilities. Many of the giant clusters could be satellites in this case, forming outside of the disk, and then the whole process of thick disk formation could be more irregular and more violent than our sample indicates.

Based on observations with the NASA/ESA Hubble Space Telescope, obtained at the Space Telescope Science Institute, which is operated by the Association of Universities for Research in Astronomy, Inc., under NASA contract NAS 5-26555. D.M.E. thanks Vassar College for a publication grant from the Research Committee. We are grateful to the referee for useful comments.

REFERENCES

Abadi, M., Navarro, J., Steinmetz, M., & Eke, V. 2003, ApJ, 597, 21

Aguerri, J.A.L., Balcells, M., & Peletier, R. F. 2001, A&A, 367, 428

Brook, C.B., Kawata, D., Gibson, B., & Freeman, K.C. 2004, ApJ, 612, 894

Brook, C.B., Gibson, B.K., Martel, H., & Kawata, D. 2005, ApJ, 630, 298

Brook, C., Kawata, D., Martel, H., Gibson, B., & Bailin, J. 2006, ApJ, 639, 126

Bruzual, G. & Charlot, S. 2003, MNRAS, 344, 1000

Burstein, D. 1979, ApJ, 234, 829

Burkert, A., Truran, J.W., & Hensler, G. 1992, ApJ, 391, 651

Buser, R., Rong, J., & Karaali, S. 1999, A&A, 348, 98

Calzetti, D., Armus, L., Bohlin, R. C., Kinney, A. L., Koornneef, J., & Storchi-Bergmann, T. 2000, ApJ, 533, 682

Carney, B.W., Latham, D.W., & Laird, J.B. 1989, AJ, 97, 423

Chabrier, G. 2003, PASP, 115, 763

Chen, B,. et al. 2001, ApJ, 553, 184

Chiba, M., & Beers, T.C. 2000, AJ, 119, 2843

Coe, D., Benitez, N., Sanchez, S.F., Jee, M., Bouwens, R., & Ford, H. 2006, astroph/0605262

Cohen, R.S., & Thaddeus, P. 1977, ApJL, 217, 155

Dalcanton, J., & Bernstein, R. 2002, AJ, 124, 1328

Du, C., et al. 2003, A&A, 407, 541

Efremov, Y. N. 1995, AJ, 110, 2757

Eggen, O.J., Lynden-Bell, D., & Sandage, A.R. 1962, ApJ, 136, 748

Elmegreen, D.M., Elmegreen, B.G., & Sheets, C.M. 2004a, ApJ, 603, 74

Elmegreen, D.M., Elmegreen, B.G., & Hirst, A.C. 2004b, ApJ, 604, L21

Elmegreen, B.G., & Elmegreen, D.M. 2005, ApJ, 627, 632

Elmegreen, B.G., Elmegreen, D.M., Vollbach, D.R., Foster, E.R., & Ferguson, T.E. 2005b, ApJ, 634, 101

Elmegreen, D.M., Elmegreen, B.G., Rubin, D.S., & Schaffer, M. 2005a, ApJ, 631, 85

Elmegreen, D.M., Elmegreen, B.G., Ravindranath, S., & Coe, 2006, in preparation for ApJ

Freeman, K.C. 1987, ARAA, 25, 603

Freeman, K.C. & Bland-Hawthorn, J. 2002, ARAA, 40, 487

Fuchs B., Dettbarn C., Jahreis, F., Wielen R. 2001, in Dynamics of Star Clusters and the Milky Way, eds. S. Deiters, B. Fuchs, A. Just, R. Spurzem, & R. Wielen, ASP Conf. Ser. Vol. 228, Astron. Soc. Pac., San Francisco, p. 235

Furhmann, K. 1998, A&A, 338, 161

Gilmore, G., & Reid, N. 1983, MNRAS, 202, 1025

Gilmore, G., Wyse, R. F. G., & Jones, J. B. 1995, AJ, 109, 1095

Gilmore, G., Wyse, R.F.G., & Norris, J.E. 2002, ApJL, 574, 39

Governato, F. 2004, ApJ, 607, 688

Immeli, A., Samland, M., Gerhard, O., & Westera, P. 2004a, A&A, 413, 547

Immeli, A., Samland, M., Westera, P., & Gerhard, O. 2004b, ApJ, 611, 20

Jensen, E., & Thuan, T. 1982, ApJS, 50, 421

Jog, C. 2005, astro-ph/0508672

Kerber, L.O., Javiel, S.C., & Santiago, B.X. 2001, A&A, 365, 424

Keres, D., Katz, N., Weinberg, D.H., & Davé, R. 2004, MNRAS, 363, 2

Kroupa, P. 2002, MNRAS, 330, 707

Larsen, J.A., & Humphreys, R.M. 2003, AJ, 125, 1958

Leitherer, C., Li, I.-H., Calzetti, D., & Heckman, T. M. 2002, ApJS, 140, 303

Madau, P. 1995, ApJ, 441, 18

Mihos, J. C., Walker, I.R., Hernquist, L., Mendes de Oliveira, C. & Bolte, M. 1997, ApJL, 447, 87

Morrison, H.L., Miller, E.D., Harding, P., Stinebring, D.R., & Boroson, Todd A. 1997, AJ, 133, 2061

Mould, J. 2005, AJ, 129, 698

Murali, C., Katz, N., Hernquist, L., Weinberg, D.H., & Davé, R. 2002, ApJ, 571, 1

Noguchi, M. 1999, ApJ, 514, 77

Ojha, D.K. 2001, MNRAS, 322, 426

Papovich, C., Dickinson, M., Giavalisco, M. 2005, ApJ, 631, 101

Pardi, M.C., Ferrini, F., & Matteucci, F. 1995, ApJ, 444, 207

Pohlen, M., Dettmar, R.-J., Lutticke, R., & Schwarzkopf, U. 2000, A&AS, 144, 405

Pohlen, M., Balcells, M. Lütticke, R. & Dettmar, R.-J.2004, A&A, 422, 465

Quinn, P.J., Hernquist, L., & Fullagar, D.P. 1993, ApJ, 403, 74

Reshetnikov, V.P., Dettmar, R.J., & Combes, F. 1997, A&A, 399, 879

Robin, A. C. Haywood, M., Creze, M., Ojha, D.K., & Bienayme, O. 1996, A&A, 305, 125

Rowan-Robinson, M. 2003, MNRAS, 345, 819

Seigel, M. H., Majewski, S. R., Reid, I. N., & Thompson, I. B. 2002, ApJ, 578, 151

Seth, A.C., Dalcanton, J.J., & de Jong, R. S. 2005, AJ, 130, 1574

Sommer-Larsen, J., Götz, M., & Portinari, L. 2003, ApJ, 596, 47

Spergel, D.N., et al. 2003, ApJS, 148, 175

Stark, A.A., & Brand, J. 1989, ApJ, 339, 763

Tsikoudi, V. 1979, ApJ, 234, 842

van der Kruit, P., Jimenez-Vicente, J., Kregel, M., & Freeman, K. 2001, A&A, 379, 374

van der Kruit, P. & Searle, L. 1981a, A&A, 95, 105

van der Kruit, P. & Searle, L. 1981b, A&A, 95, 116

van Dokkum, P., Peletier, R., de Grijs, R., & Balcells, M. 1994, A&A, 286, 415

Velazquez, H., & White, S.D.M. 1999, MNRAS, 304, 254

de Vaucouleurs, G., de Vaucouleurs, A., Corwin, H., Buta, R., Paturel, G., & Fouque, P. 1991, Third Reference Catalogue of Galaxies, New York: Springer-Verlag

Walker, I.R., Mihos, J. C. & Hernquist, L. 1996, ApJ, 460, 121

Westera, P., Samland, M., Buser, R., & Gerhard, O.E. 2002, A&A, 389, 761

Wielen, R., & Fuchs, B. 1985, in IAU Symp. 106, The Milky Way Galaxy, ed. H. van Woerden, R.J. Allen, & W.B. Burton (Dordrecht: Reidel), 481

Wyse, R. 2004, in The Local Group as an Astrophysical Laboratory, ed. M. Livio (Cambridge: Cambridge Univ. Press), astro-ph/0402636

Wyse, R., et al. 2006, ApJ, 639, L13

Yoachim, P. & Dalcanton, J.J. 2005, ApJ, 624, 701

Yoachim, P. & Dalcanton, J.J. 2006, AJ, 131, 226

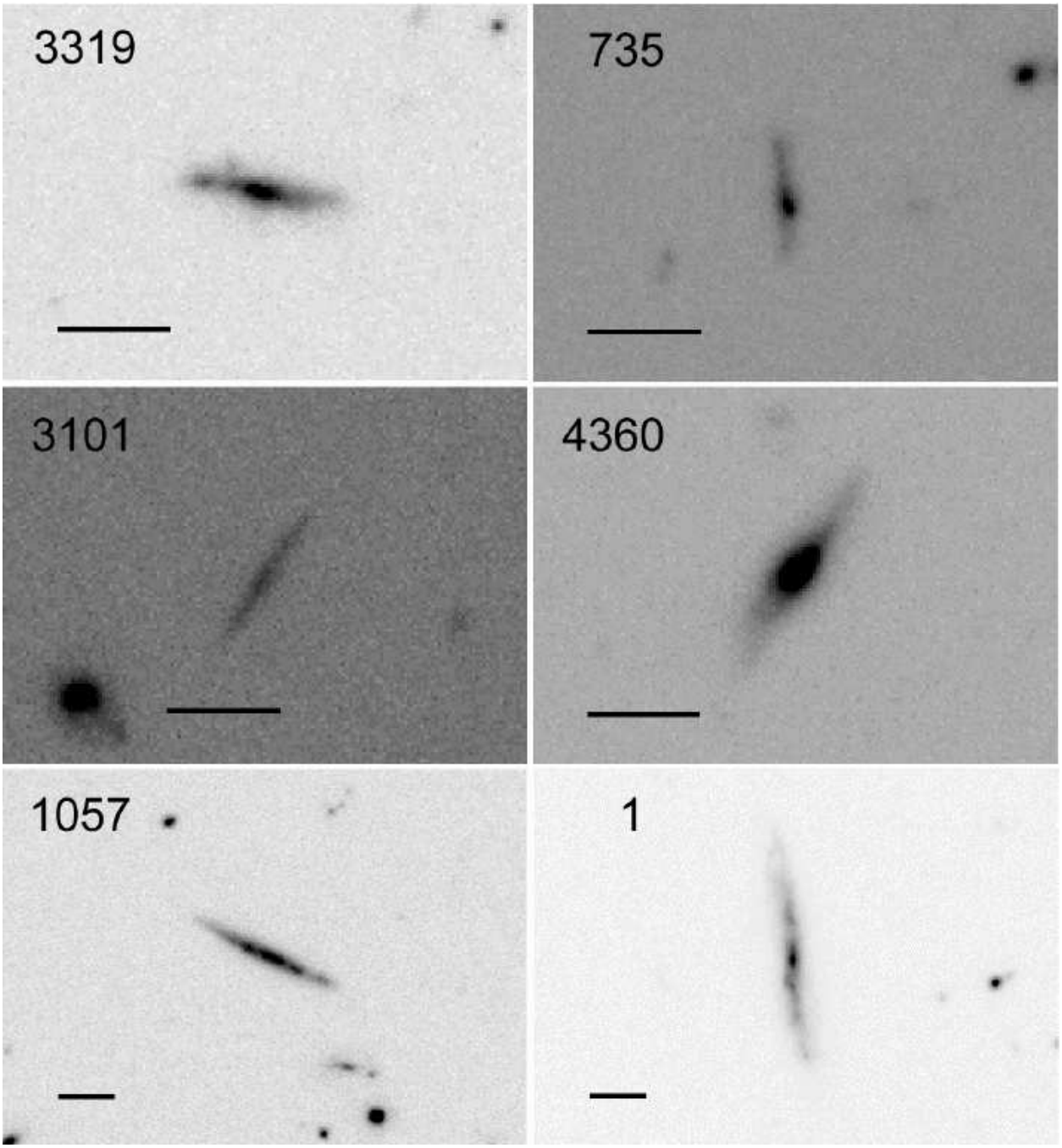

Fig. 1.— Sample edge-on spiral galaxies with UDF catalog numbers indicated. The length bars in the lower left are 1 arcsec.

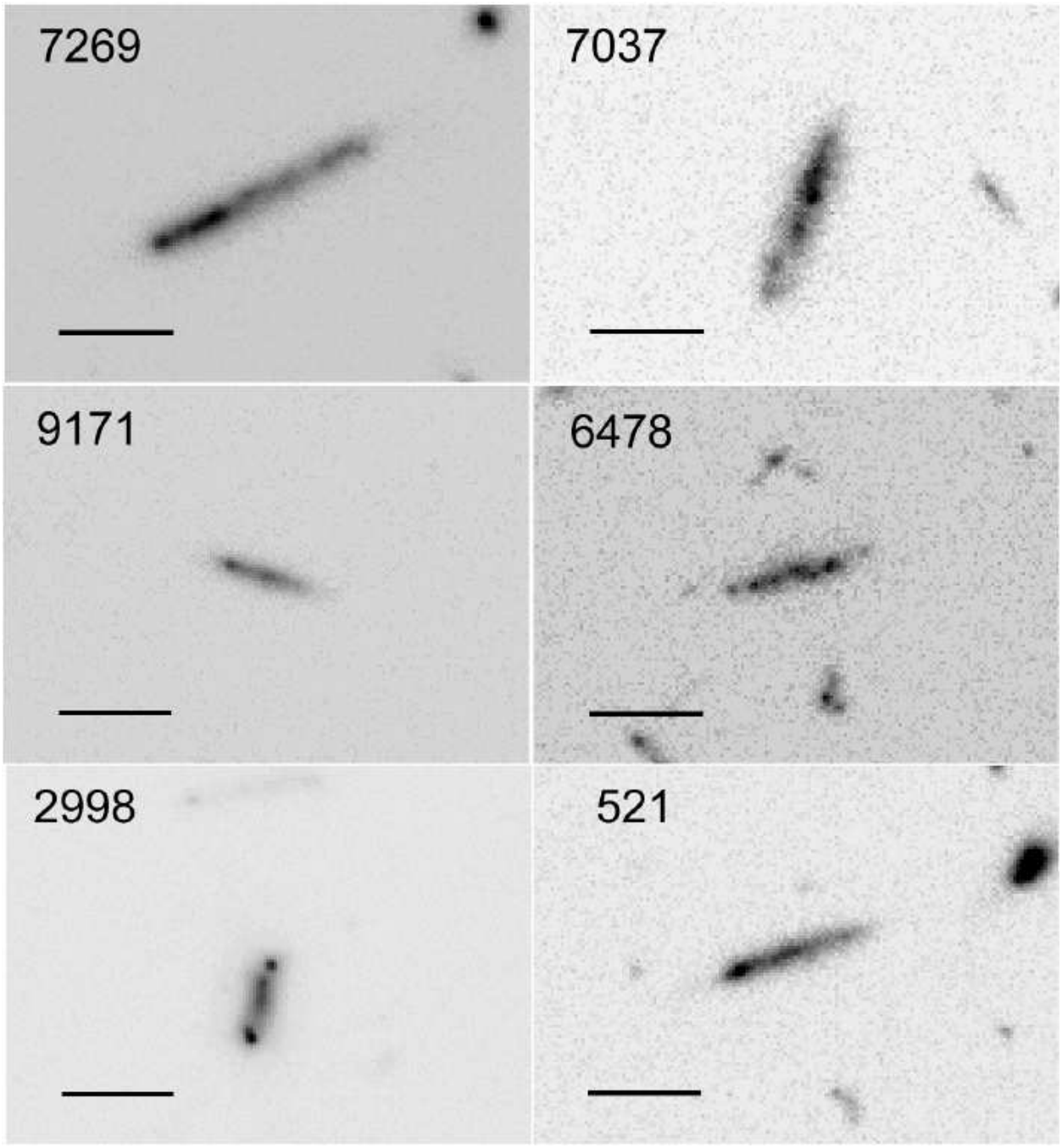

Fig. 2.— Sample chain galaxies with UDF numbers and 1 arcsec scale indicators. Chain galaxies contain prominent clumps and no central red bulge.

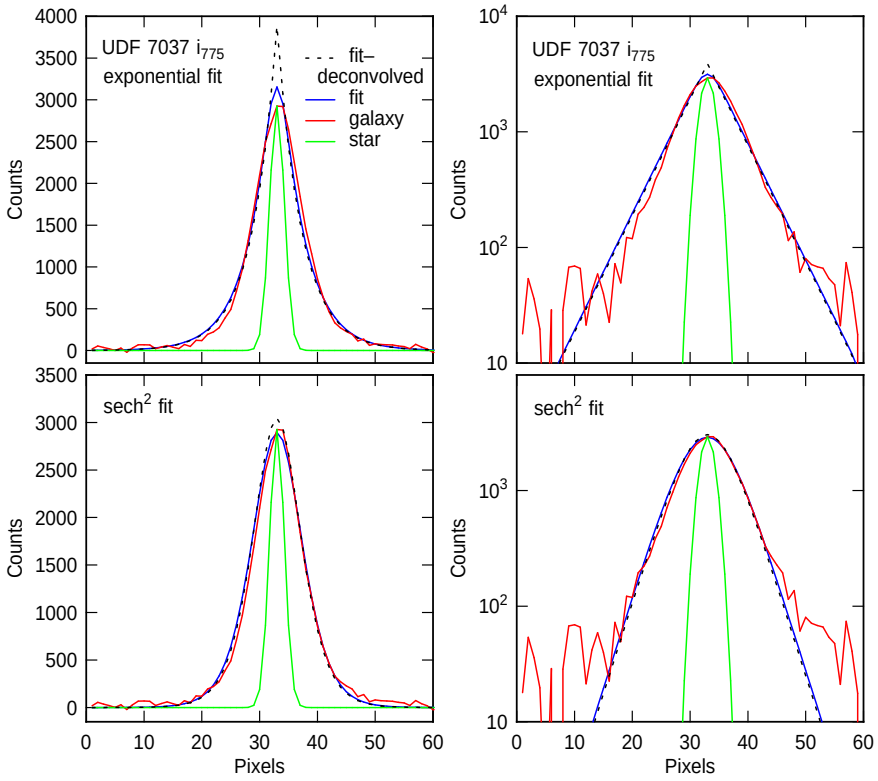

Fig. 3.— Perpendicular profiles through the chain galaxy UDF 7037 in the i_{775} band along with exponential fits (top) and sech^2 fits (bottom). The thin green profile is the average from 15 stars. The curve with slight noise (red) is the galaxy profile, the smooth dashed line (black) is the intrinsic profile with the star deconvolved (from the fit), and the solid line (blue) is the convolution of the star and the intrinsic profile, fitted to the galaxy. Colors are shown in the electronic version of this manuscript.

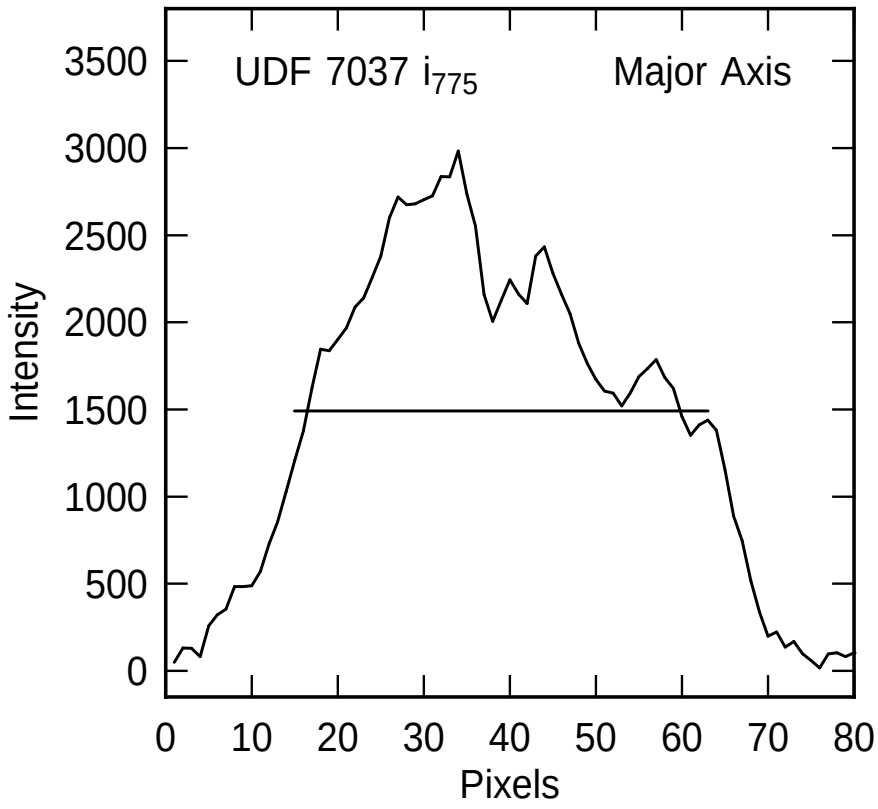

Fig. 4.— Parallel profile through the chain galaxy UDF 7037 in the i_{775} band. The clumps in the image in Fig. 2 are the large peaks in the profile. The horizontal line is the end-to-end length of the galaxy used in Sect. 3.7 and in Figs. 16 and 17.

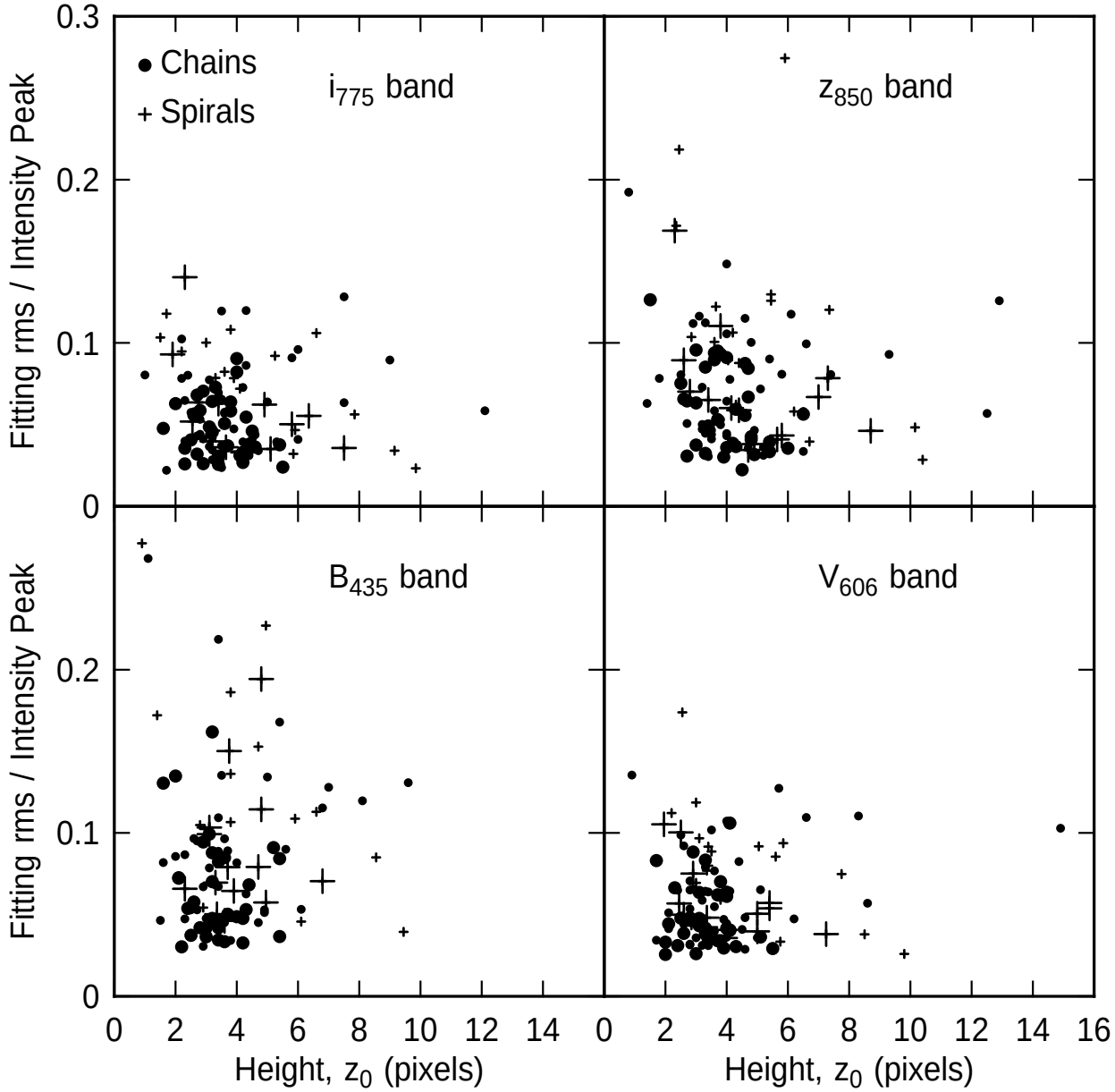

Fig. 5.— Ratios of the rms deviations between observed profiles and the fitted profiles to the peak intensities in the observed profiles are plotted versus the derived sech^2 heights in pixels. The typical relative accuracy of the fit is $\sim 5\%$. The relative accuracy of the scale heights is $\sim 20\%$ (see text). The large symbols are the best case galaxies.

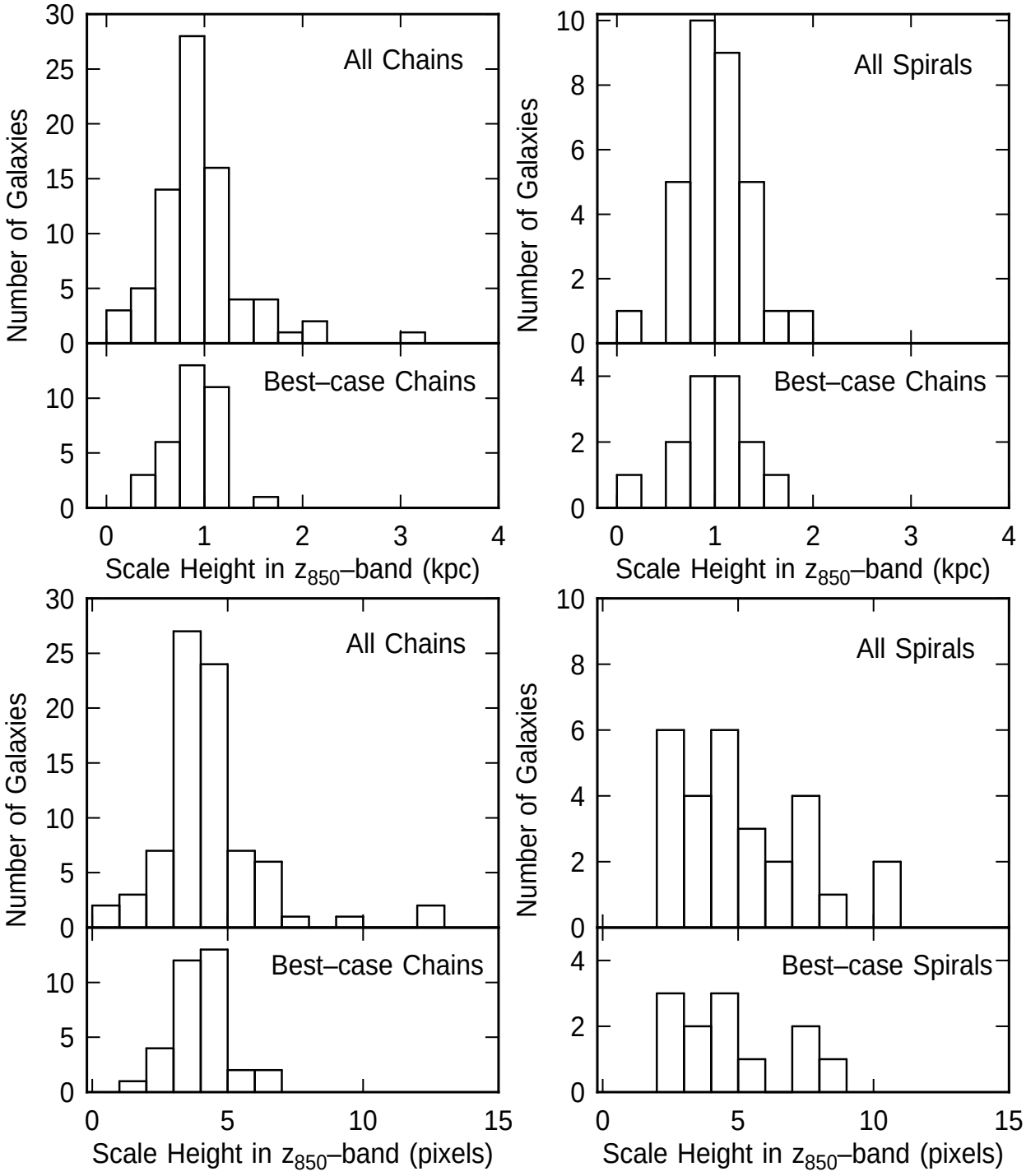

Fig. 6.— The distribution of fitted scale heights, in pixels for the bottom panels and in kpc for the top panels, assuming photometric redshifts. The distributions for the best case galaxies are plotted separately. The chain and spiral galaxy scale heights cluster around 0.9-1 kpc.

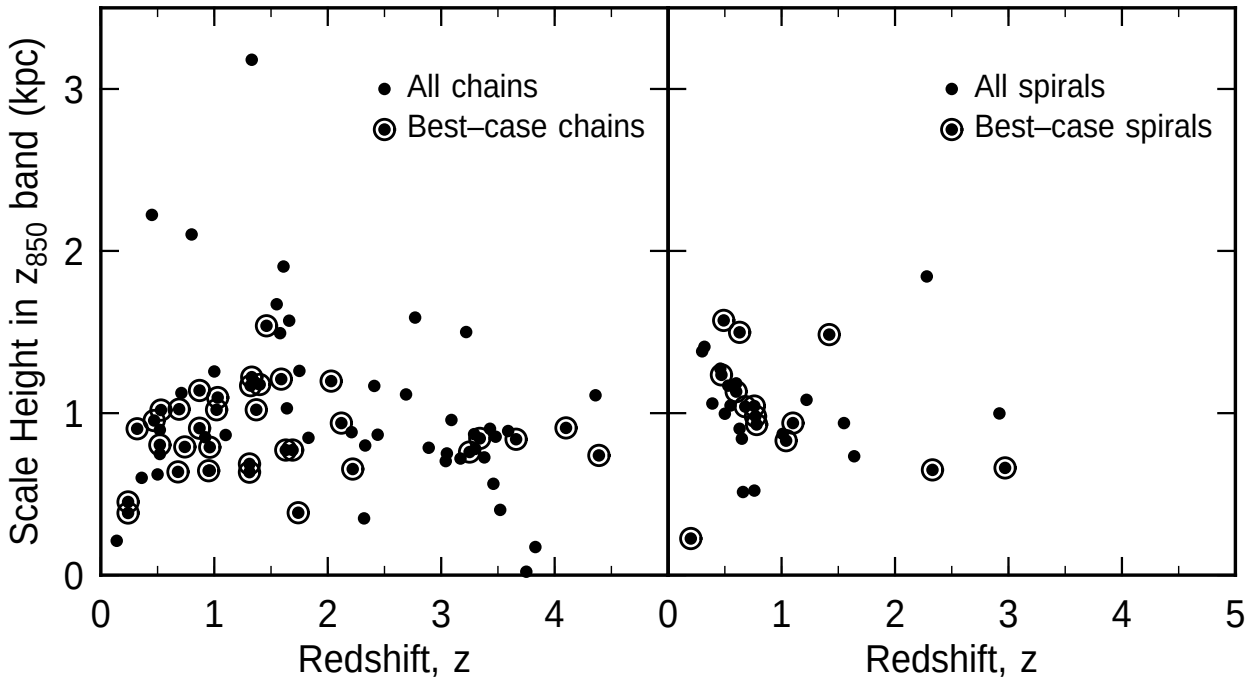

Fig. 7.— The z_{850}-band scale height in kpc is shown versus the redshift. There is no systematic trend except for an excess of small heights at the lowest redshift.

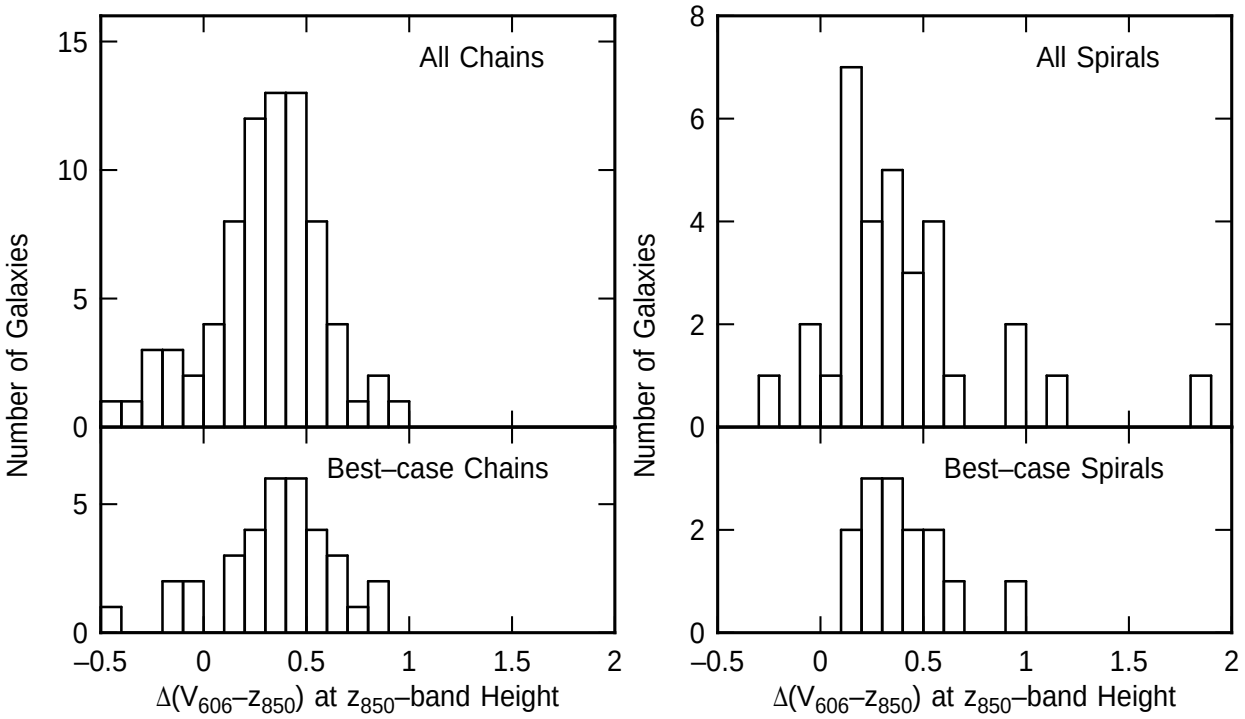

Fig. 8.— The distribution of color difference between the midplane and one z_{850}-band scale height. There is a $\sim 0.3 - 0.4$ mag reddening with height.

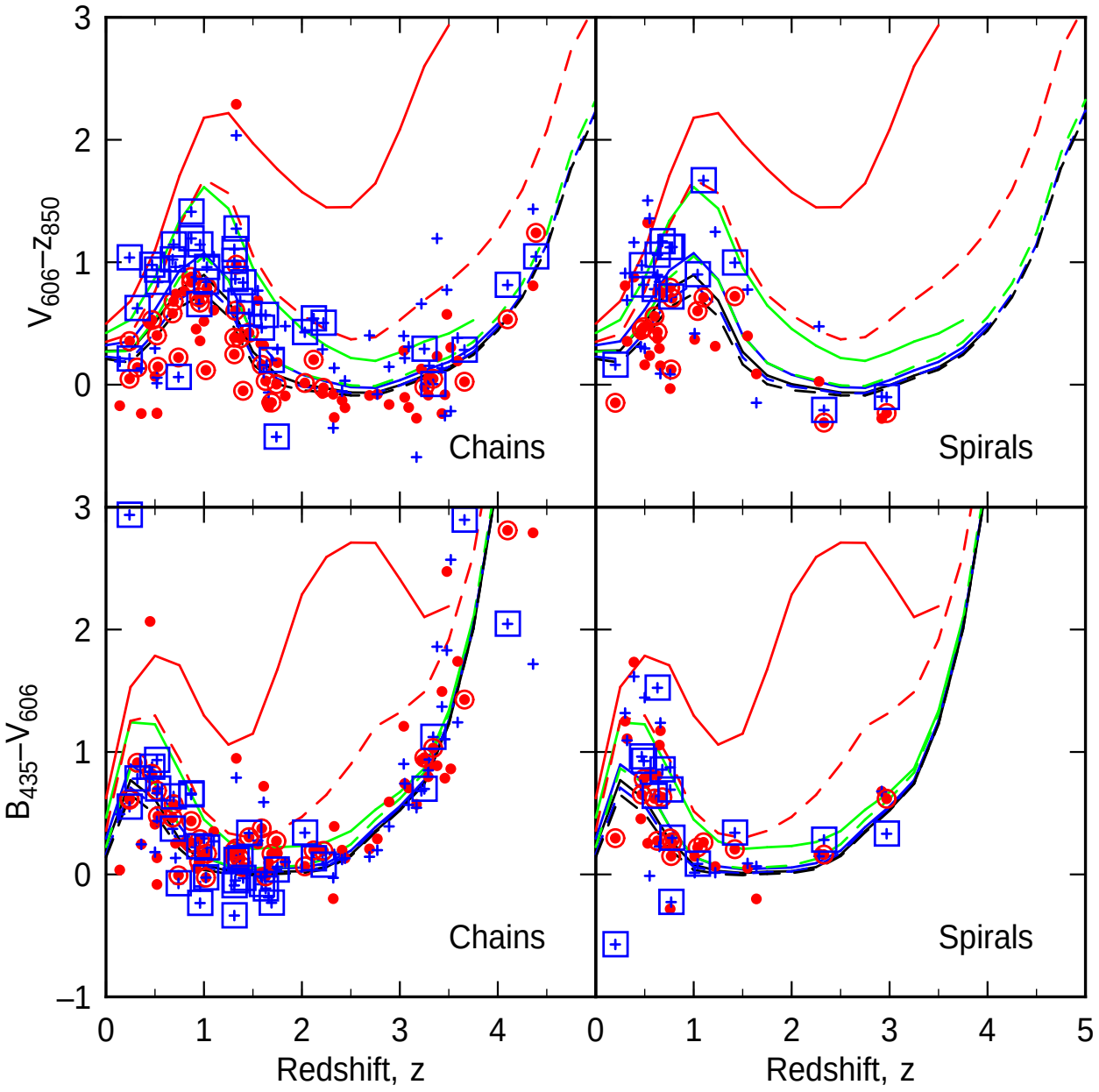

Fig. 9.— Color versus redshift with superposed curves calculated from redshifted stellar population models. The dots and filled circles (red in electronic version) are the midplane values, with filled circles for the best cases. The plus symbols and filled squares (blue) are the off-plane values, with filled squares the best cases. The solid lines are for a star formation duration of 1 Gy and the dashed lines are for a duration of 0.5 Gy. The star formation rate is assumed to decay exponentially during these times, with decay times equal to 0.1 Gy (red curves), 0.3 Gy (green), 1 Gy (blue), and infinity (continuous star formation, black curves), increasing as the models get bluer (lower in the figure). The best fit curves suggest there is significant active star formation in all of the galaxies. The redder off-plane $V_{606}-z_{850}$ colors fit to models with slightly less current star formation. These colors are consistent with thick disk luminous ages (i.e., weighted toward these restframe uv bands) of around 1 Gy and either continuous star formation or slowly declining star formation.

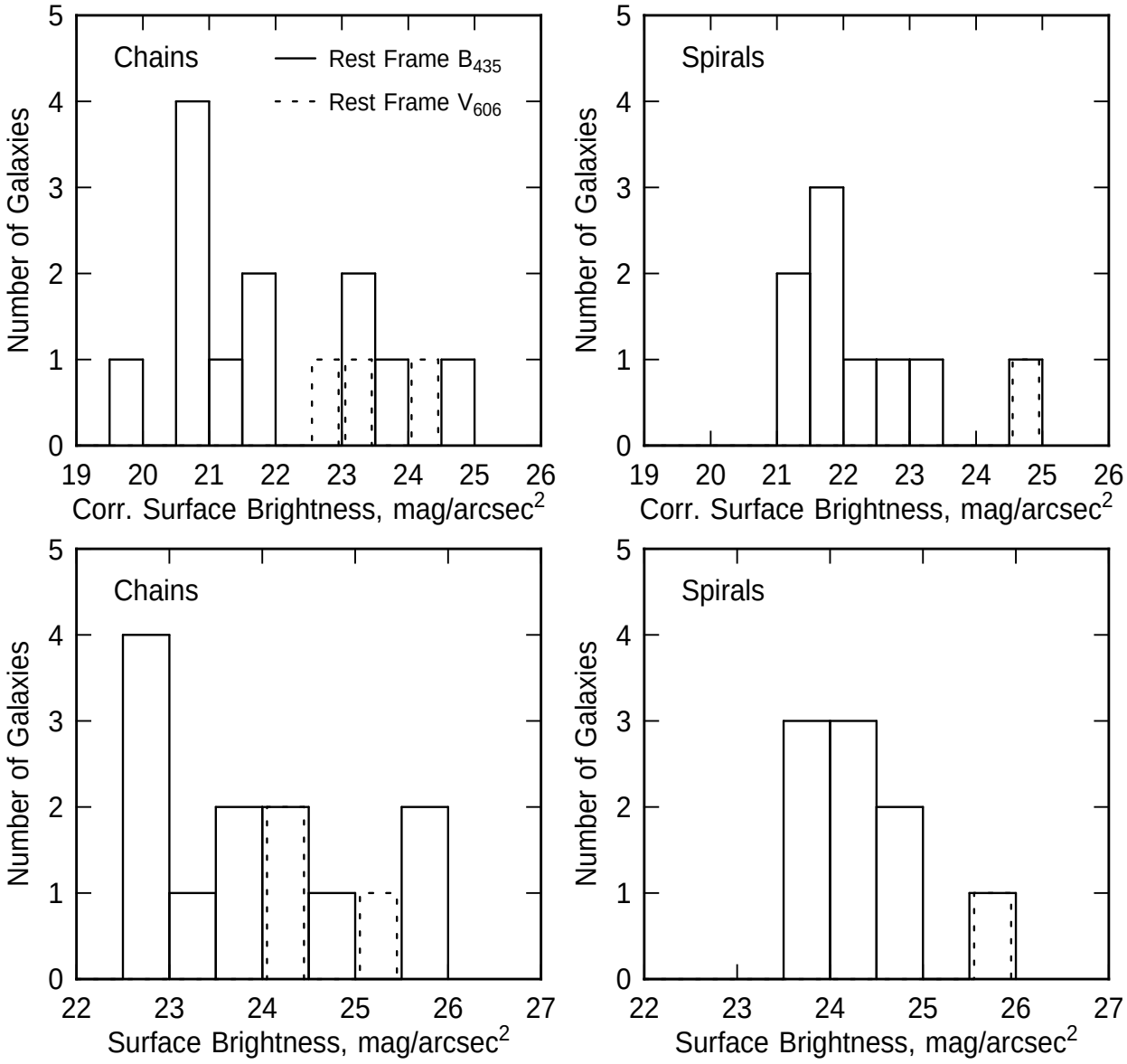

Fig. 10.— Observed (bottom) and corrected restframe (top) surface brightnesses in B_{435} and V_{606} (dashed lines) at the midplanes of the best case galaxies. The surface brightness correction is by interpolation from the ACS bands to the restframe band, and by subtraction of $10 \log (1 + z)$ to account for cosmological dimming. The midplane values come from the sech^2 fits.

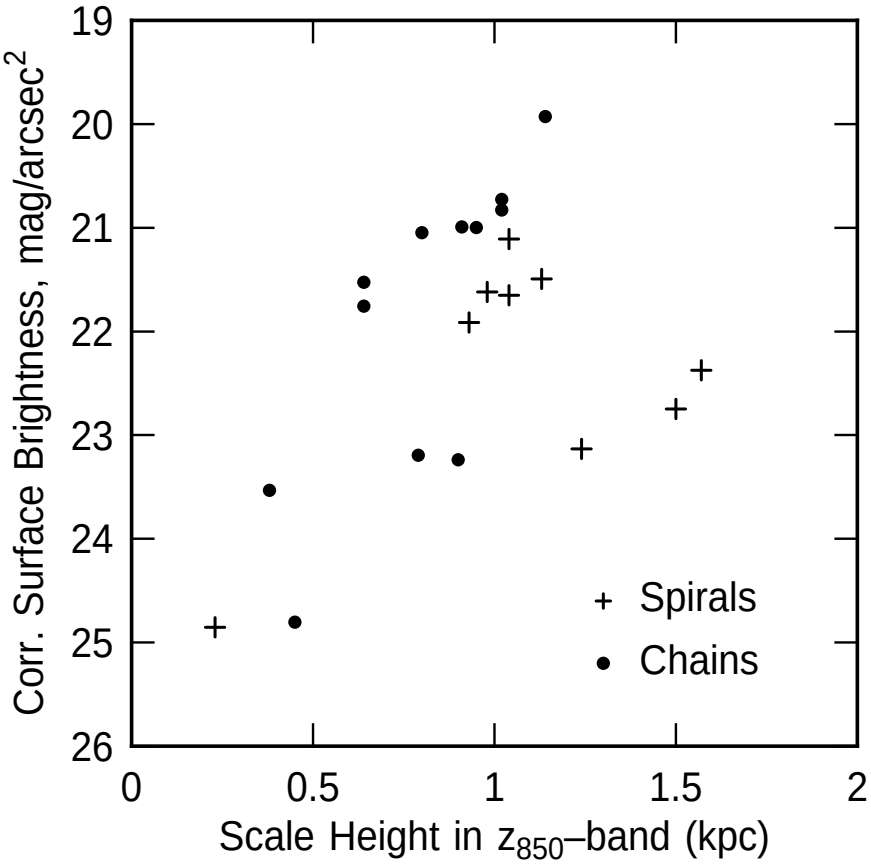

Fig. 11.— Corrected restframe midplane B_{435} surface brightness versus the z_{850}-band scale height. There is a slight correlation in the sense that the larger galaxies have brighter intrinsic midplane intensities.

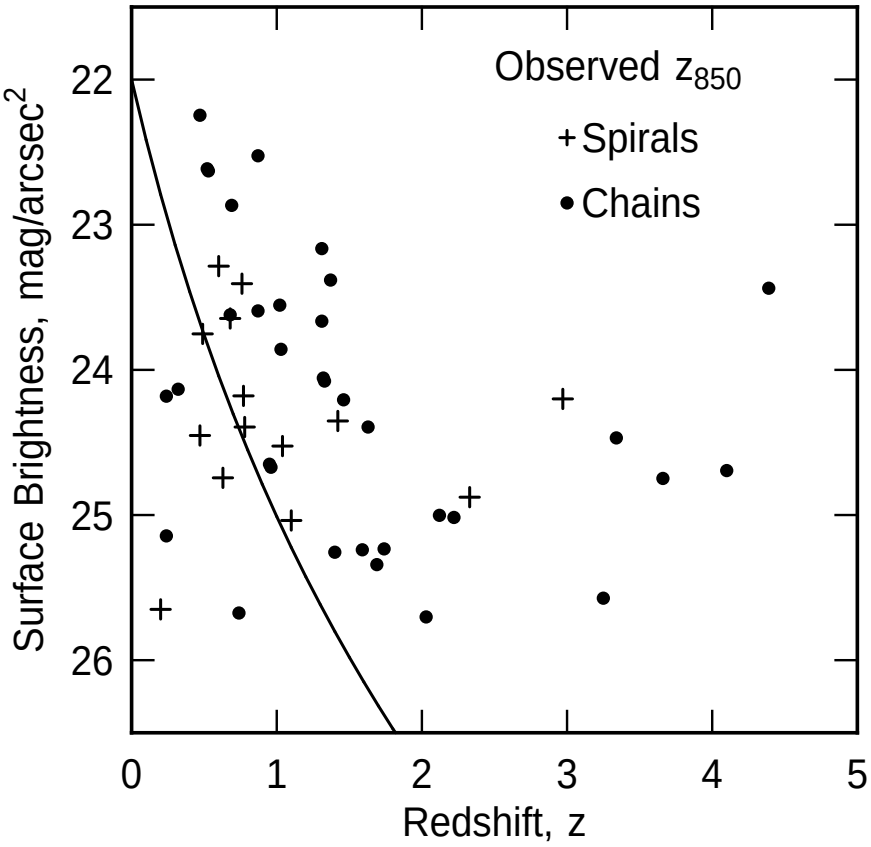

Fig. 12.— The fitted midplane surface brightness in z_{850} band, uncorrected to the restframe and uncorrected for surface brightness dimming, is shown versus the redshift. This observed surface brightness is compared to redshifted stellar population models in the text in order to estimate the mass surface density of the disk. The curve is the $(1+z)^{-4}$ cosmological dimming function with arbitrary zero point.

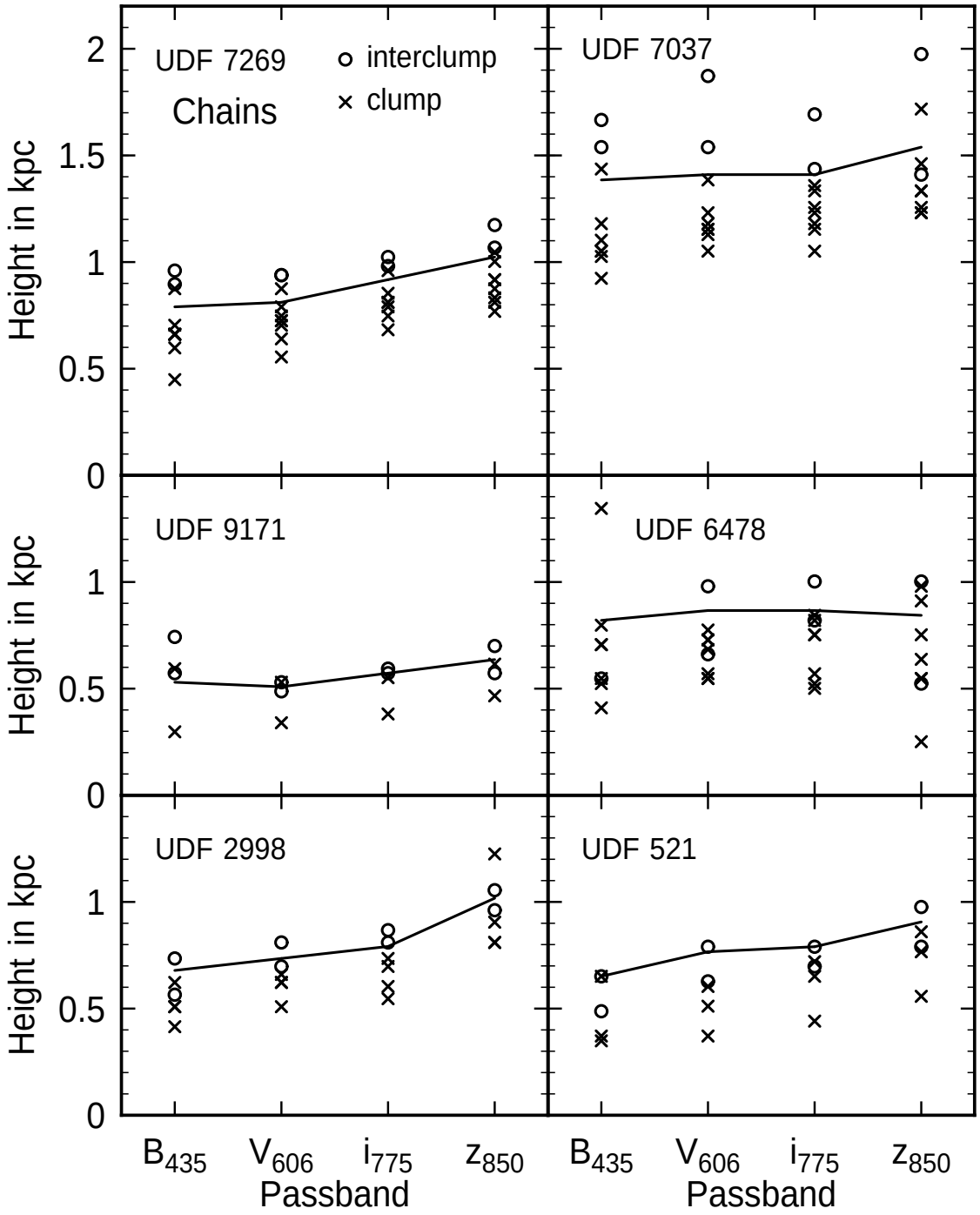

Fig. 13.— The sech^2 scale heights of the clumps (x-marks), interclump emission (circles), and average disks (solid lines) are shown versus bandpass for the six chain galaxies illustrated in Fig. 2. The interclump emission has about the same thickness as the whole galaxy, but the clumps are $\sim 20\%$ smaller. This similarity in size suggests that the stellar disk is built-up by the dissolution of stellar clumps. The slight upward trend with longer wavelength is the same reddening with height shown in Fig. 7.

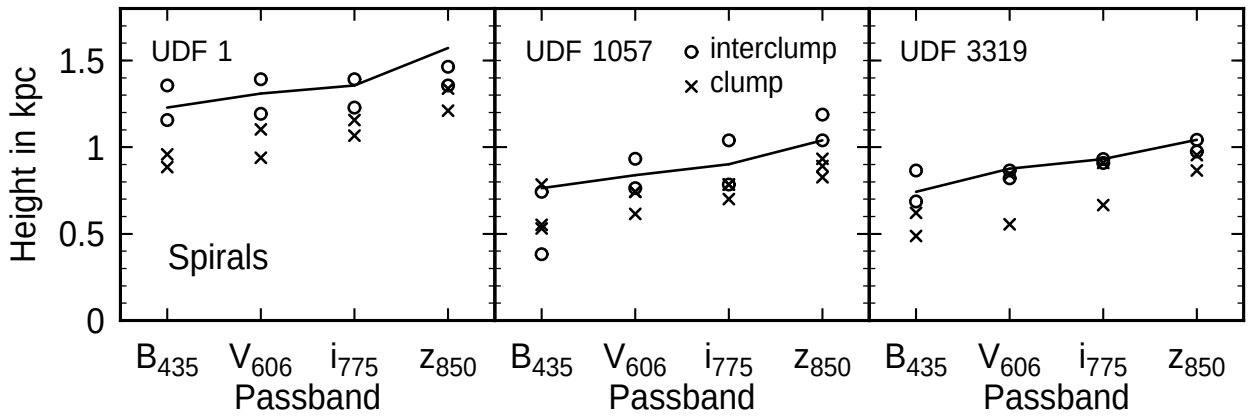

Fig. 14.— The sech^2 scale heights of the clumps (x-marks), interclump emission (circles), and average disks (solid lines) are shown versus bandpass for three spiral galaxies illustrated in Fig. 1.

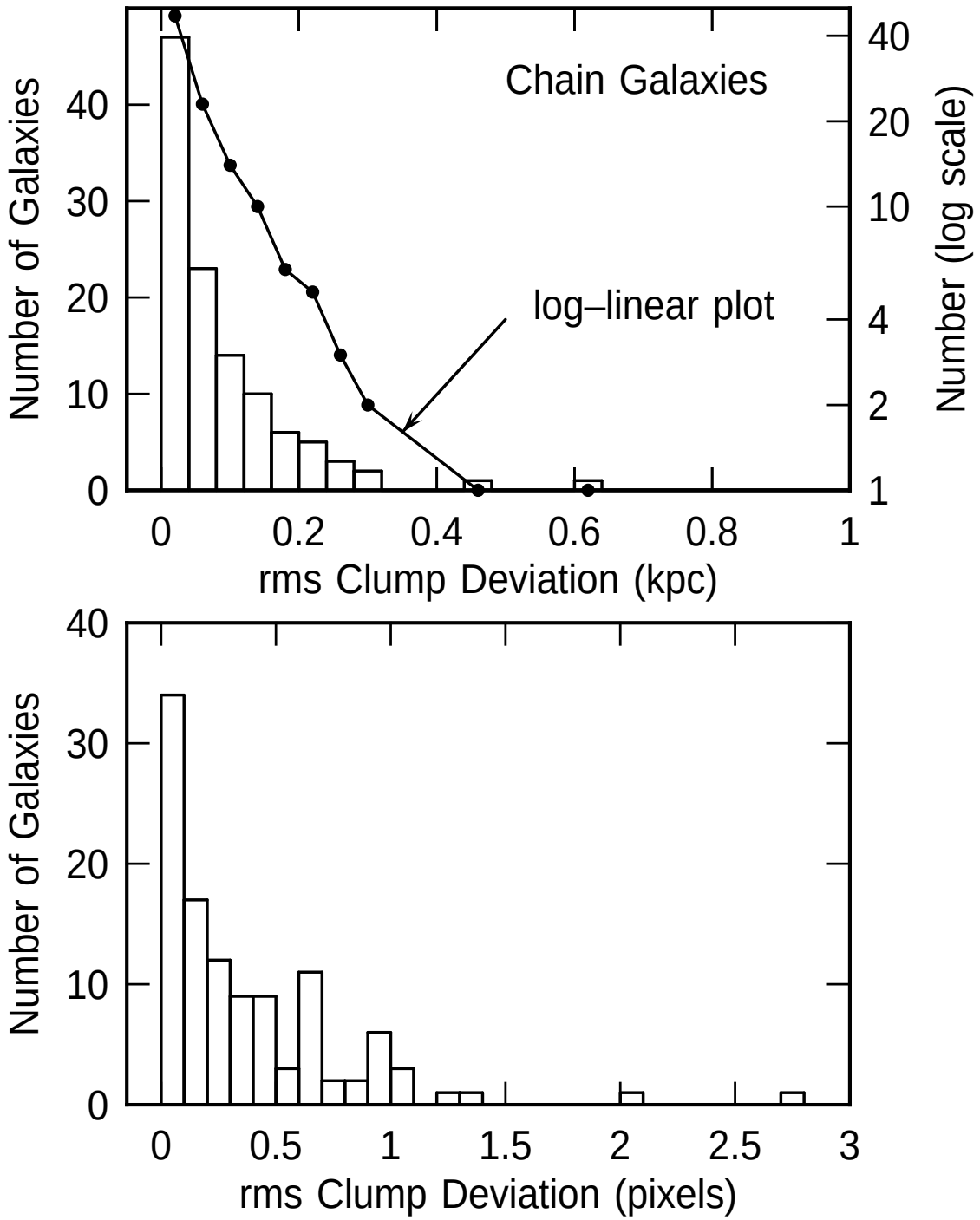

Fig. 15.— The distribution of rms deviation of the clump centers around the average midplane line defined by these centers, for 431 clumps in 112 chain galaxies from our UDF catalog. The deviations are shown in pixels at the bottom and in kpc at the top. The line at the top uses the right-hand logarithmic scale. The clump deviations from the midplane are very small, suggesting the clumps formed there and did not enter the galaxy from outside.

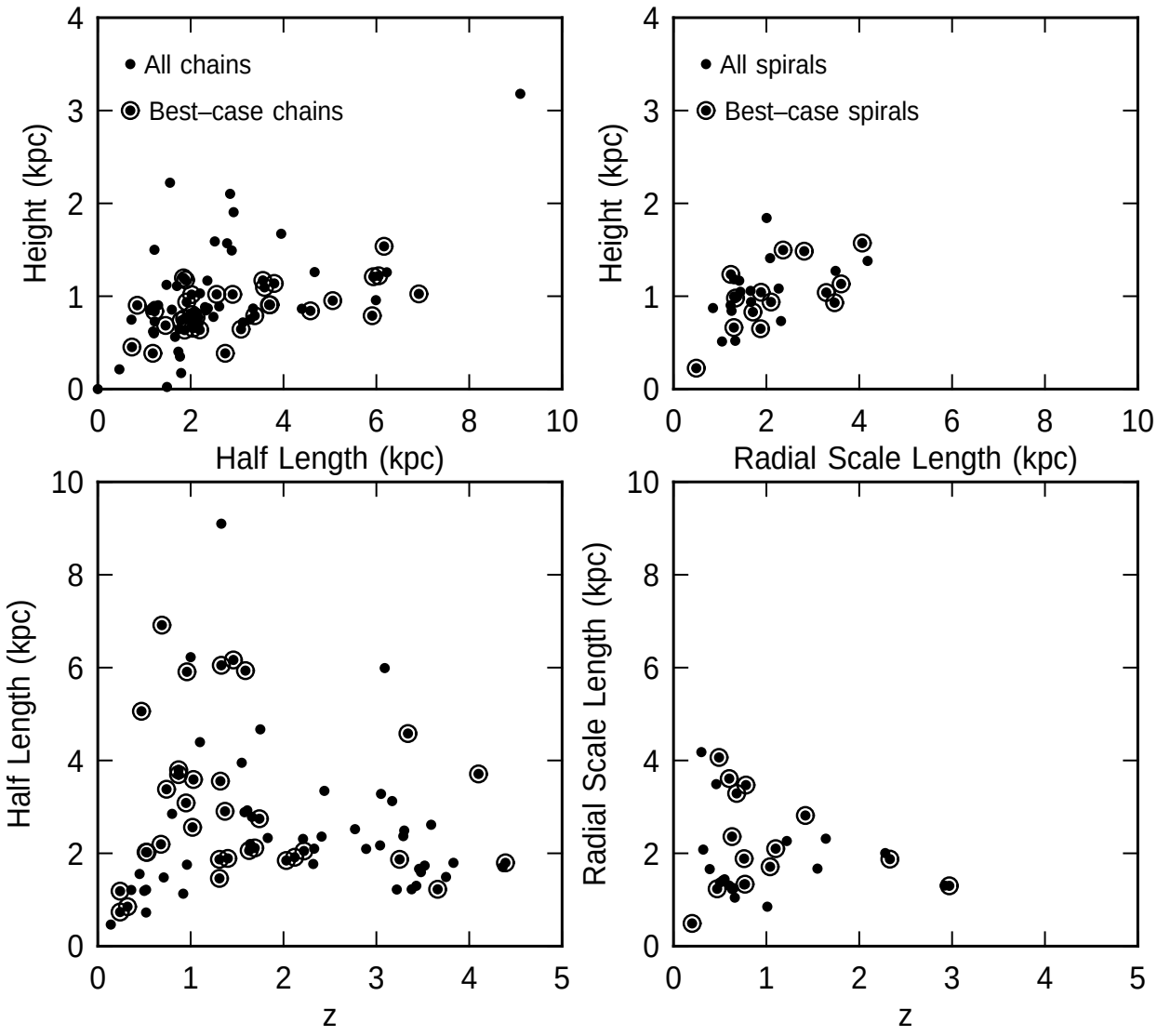

Fig. 16.— The radial scale lengths for spirals (right) and the half-lengths for chains (left), in kpc, are shown versus the redshift in the lower panels. These are for the z_{850} band. The $sech^2$ heights are plotted versus the radial lengths in the top panels. There is a slight correlation between the lengths and widths, which makes the ratio of axis cluster around 3:1 or 2:1 (Fig. 17).

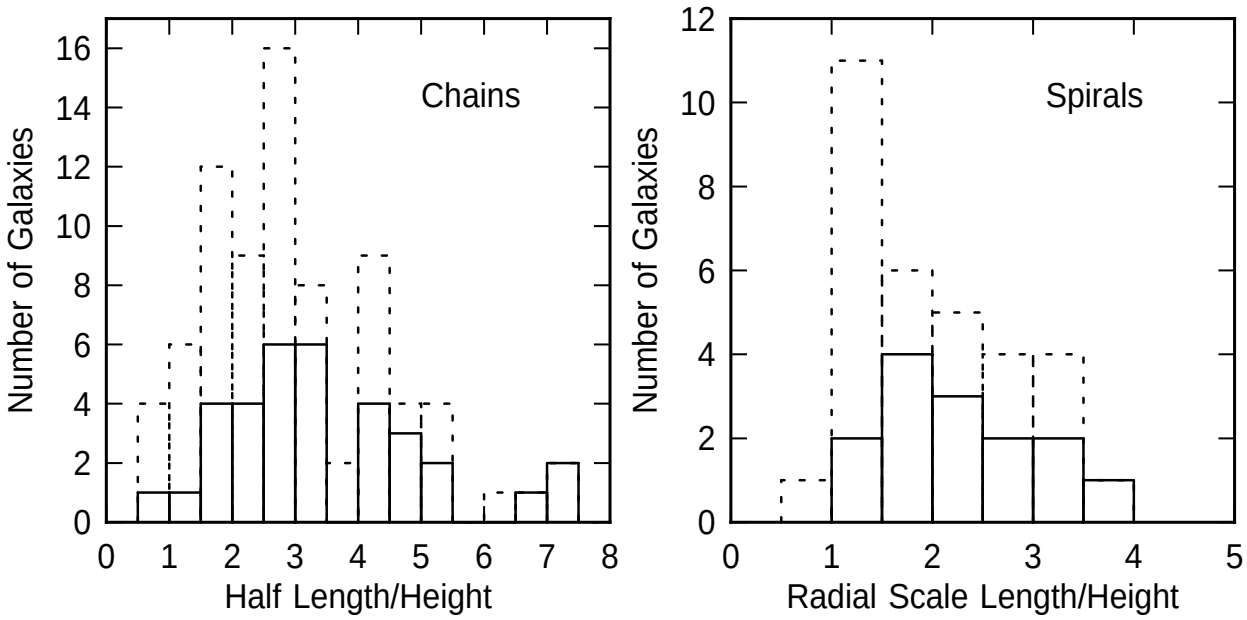

Fig. 17.— The distribution of the ratio of radial scale length (spirals) or half-length (chains) to perpendicular sech^2 height is shown for the best-case galaxies with solid lines and for all of the galaxies with dashed lines. The measurements are for the z_{850} band. Two chain galaxies with less certain measurements are off scale on the right with ratios of ~ 10 and ~ 68. The average ratio for the best-case spirals is 2.3 ± 0.7, and the average for the best-case chains is 3.4 ± 1.6.

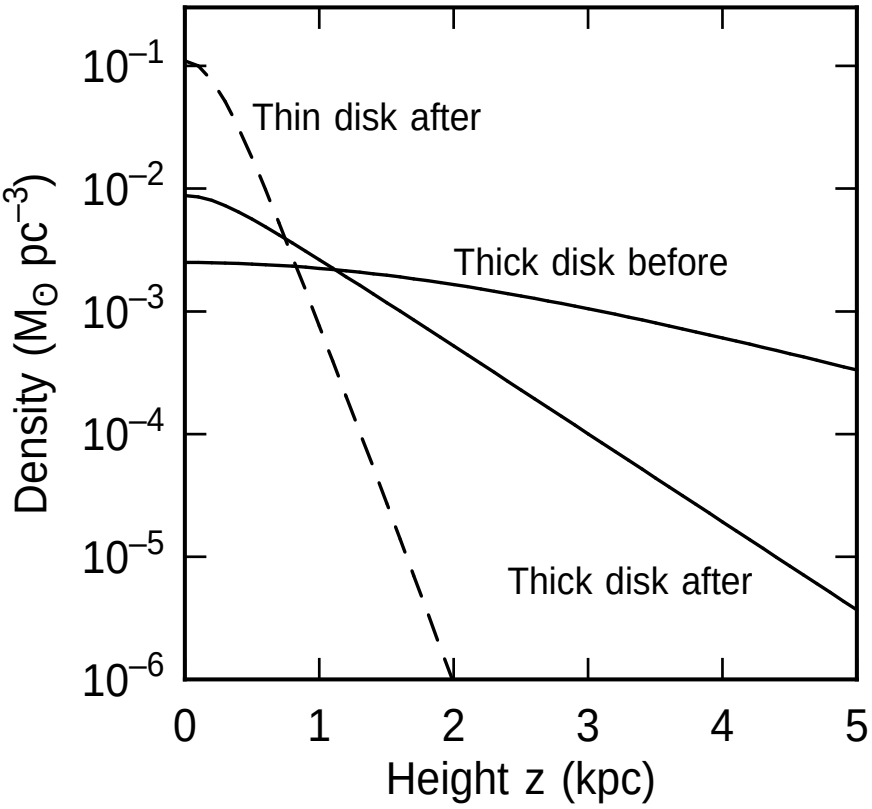

Fig. 18.— Model illustrating the vertical contraction of an initial thick disk after the addition of a massive thin disk component. The thick disk has a constant mass column density of 15 $M_\odot$ pc^{-2} but its velocity dispersion increases adiabatically during the contraction. Before the addition of the thin disk, the thick disk has a sech^2 scale height of 3 kpc and a vertical velocity dispersion of 25 km s^{-1}. The thin disk column density is 70 $M_\odot$ pc^{-2} and its velocity dispersion is 18.5 km s^{-1}. The initial thick disk shrinks down to a smaller thick disk component with a $1/e$ half-thickness of 875 pc, a vertical velocity dispersion of 38 km s^{-1}, and a midplane mass ratio to the thin disk of 8%. This final state resembles the old thin disk and the thick disk of the Milky Way, suggesting that the initial thick disk had to be ~ 3 kpc in scale height – much larger than what we observe in the UDF.